A numerical study on predicting bond-slip relationship of reinforced concrete using surface based cohesive behavior

Minhajul Bari Prince
Bangladesh University of Engineering and Technology, Dhaka, Bangladesh
minhajulbariprince@gmail.com, https://orcid.org/0009-0002-9822-6157

Debasish Sen
Ahsanullah University of Science and Technology, Dhaka, Bangladesh
debasish.ce@aust.edu, https://orcid.org/0000-0001-6375-4596

Citation: Prince, M. B., Sen,, D., A numerical study on predicting bond-slip relationship of reinforced concrete using surface based cohesive behavior, Frattura ed Integrità Strutturale, 69 (2024) 154-180.

Received: 23.03.2024
Accepted: 07.05.2024
Published: 10.05.2024
Issue: 07.2024

KEYWORDS. Bond-slip model, Pullout test, Surface-to-surface cohesive behavior, FEM, Bond stress-slip curve.

INTRODUCTION

Composite action between reinforcement and surrounded concrete is required for successful load transfer in structures. The interaction behaviour that ensures this act is called a bond. The pullout test is performed by embedding reinforcement concentrically or eccentrically into a pullout specimen (i.e., a concrete cube, a cylinder) to investigate the bond-slip behaviour of steel in concrete. Sometimes, transverse reinforcement could be placed inside specimens to consider the confinement action of concrete. Factors like concrete cover-to-bar diameter ratio, the tensile strength of concrete, released fracture energy during cracking, rib profile, strength and stiffness of rebar and concrete, and stiffness of transverse reinforcement are the most important in bond mechanism [1]. When reinforcement is pulled by tension, the chemical adhesion of concrete starts to break. As a result, different modes of failure patterns (i.e., pullout, splitting, and a combination of both pullout and splitting) are observed. Therefore, pullout tests need to be performed to

learn reinforced concrete specimens' failure patterns and bond-slip relationships. However, a parametric study needs to change various specimen parameters, such as concrete compressive strength, concrete cover, bar diameter, bonded length, etc. Therefore, the experiment had to be performed several times, which was time-consuming and costly. In addition, the bond-slip curve and failure pattern at peak bond stress, crack propagation mechanism and contact status throughout the pullout loading need to be studied to understand bond-slip behaviour in reinforced concrete. However, these outputs could not be extracted from the experiment.

Therefore, finite element analysis is needed to observe bond-slip behaviour more explicitly. Modelling the interaction between reinforcement and concrete is the most crucial factor affecting the bond-slip relationship. Analytical models can assist with interaction modelling. In this context, researchers developed analytical models for predicting bond strength by regression analysis [2-12]. However, the scope of using the proposed formula suggested by researchers must be studied before use. A brief literature study of the available proposals for predicting bond strength and their corresponding scopes is shown in Tab. 1. Nevertheless, several previous studies focused on developing finite modelling of the bond-ship behaviour of reinforced concrete and comparing finite element analysis results with the experimental results to learn the effectiveness of their finite element model. Burdziński and Niedostatkiewicz [13] performed pullout tests experimentally with C35/45-grade concrete and B500SP reinforcement with three different bar diameters of 10, 12 and 16 mm. They numerically model specimens using the finite element method in ABAQUS software. The concrete damage plasticity model was used to model concrete, and contact cohesive behaviour was used to model the interface of concrete and rebar. The bond-slip curve reflected the experimental results correctly and started to deviate after reaching peak bond stress. They focused on the calibration of FE models to match the experimental results. Abbas et al. [14] performed finite element analysis in ANSYS software and compared the FEM bond-slip curve with the experiment. Their bond-slip curve showed that the stiffness did not reflect the experimental results correctly. Moreover, specimens with bonded lengths equal to five times the diameter show a lower bond strength than an experiment. They found that the difficulties in predicting the stiffness of the interface component could be attributed to the mismatches (errors) between the experimental and predicted FE analysis results. Beliaev et al. [15] compared the outcomes of the experiments with the different FE methods used to model the pullout of the steel rebar from the concrete block. They suggested that concrete with nonlinear material modelling and using cohesive behaviour as the interaction between reinforcement and concrete exhibits correct bond-slip behaviour. Murcia-Delso [16] developed a new interface model with four nodes (two connected to bonded rebar and two to bonded concrete) for simulating the bond-slip relationship between reinforcement and concrete. After calibration, the interface model successfully reflects the experiment result in well-confined concrete. However, the stiffness varied for some specimens from the experiment. Cairns [17] studied the shortcomings of the bond-slip parameters of fib Model Code 2010 for plain reinforcement and proposed an improved model. The study found that the proposed fib Model Code 2010 equation to calculate maximum bond stress is conservative. Tabatabaei et al. [18] used a ring contact element as an elastoplastic cylinder contact element to generate an interface between concrete and reinforcement, representing a bond-slip relationship. They calibrated with experiment values by reducing the strength of the ring contact element. They found that the slip increased with the reduction of ring element strength. Luna Molina [19] used surface-based cohesive contact behaviour to develop contact between concrete and galvanized steel and validated the bond-slip curve with experimental results. The developed model correctly reflects the peak bond stress, although the stiffness differed from the experiment. Valente [20] used surface-based interaction to model the interaction between reinforcement and concrete. The study found that the bond-slip relation of the FE model has minor stiffness anomalies and slightly overestimated bond strength and slide at peak stress.

Therefore, previous studies mainly delved into calibrating different parameters to reflect the experimental bond-slip relationship. However, a single FE analysis takes three to ten hours to complete. Calibration without proper guidelines of the value range may consume more time, leading to higher computational costs. Moreover, a reasonable initial prediction is needed before starting numerical modelling as finite element software requires some interaction value to input. Considering these aspects, this study initially predicts the failure pattern of reference specimens, and the FE modeling has been completed according to the prediction. Later, the predicted bond behaviour's effectiveness was checked by comparing the result with the reference experimental specimens [12,21]. Besides, previous studies showed a deviation of FEM stiffness from the experiment. Therefore, this study has emphasized on predicting the maximum bond stress and stiffness of the FE models.In short, the main objective of this study is to propose a well-defined FE modeling strategy in ABAQUS to predict the bond-slip relationship of reinforced concrete under the pullout test using surface-based cohesive behaviour as the interaction between reinforcement and concrete. The effectiveness of the proposed finite element modeling strategy was then studied by comparing the experimental work of Deng et al. [21] and Tang and Cheng [12] with respect to the bond-slip curve and failure pattern.

Reference	τ_{max} (SI unit)	Criteria
Model Code 2010 [2] (Pullout Failure)	$\tau_{max}=2.5\sqrt{f_c'}$	This equation is valid for pullout failure with $\frac{c}{d_B}\geq 5$
Model Code 2010 [2] (Splitting Failure)	$\tau_{max}=7.0(\frac{f'_c}{20})^{0.25}$	This equation is valid for splitting failure without confinement
Model Code 2010 [2] (Splitting Failure with confinement)	$\tau_{max}=8.0(\frac{f'_c}{20})^{0.25}$	This equation is valid for splitting failure with confinement
Sturm and Visintin [3]	$\tau_{max}=(0.0018c+0.186)f_c'$	This equation was proposed for UHPFRC. No limitation of failure pattern was found.
Esfahani and Rangan [4]	$\tau_{max}=8.6\left(\frac{c/d_B+0.5}{c/d_B+5.5}\right)f_{ct}$	The formula was proposed for high-strength concrete with compressive strength equal to or greater than 50 MPa. Moreover, $\frac{c}{d_B}\geq 1$ was another criterion, and most specimens using the regression showed failure due to bond.
Harajli et al. [5]	$\tau_{max}=2.57\sqrt{f_c'}$	This equation proposed for FRC. $\frac{c}{d_B}=3.7$ was dominant among the specimens.
Huang et al. [6]	$\tau_{max}=0.45f_c'$	Pullout failure was dominant in the specimens used to generate this equation.
Oragun et al. [7]	$\tau_{max}=0.083045\left(1.2+3\frac{c}{d_B}+50\frac{d_B}{l_B}\right)\sqrt{f'_c}$	Most of the data on which the empirical equation is based are for $\frac{c}{d_B}\leq 2.5$
Hadi [8]	$\tau_{max}=0.083045\sqrt{f_c'}\left[22.8-0.208\frac{c}{d_B}-38.212\frac{d_b}{l_d}\right]$	Splitting failure mode was the predominant type of failure of the tested specimen
Soroushian and Choi [9]	$\tau_{max}=(20-\frac{d_B}{4})\sqrt{\frac{f_c'}{30}}$	The formula was proposed for confined concrete from the partial bond pullout test. The test specimens simulated the behavior of anchored bars with $\frac{c}{d_B}=4$
Aslani and Samali [10]	$\tau_{max}=\left[0.679\left(\frac{c}{d_B}\right)^{0.6}+3.88\left(\frac{d_B}{l_B}\right)\right](f'c)^{0.55}$	The empirical formula was proposed for confined concrete. The failure pattern was not mentioned explicitly.
Xu [11]	$\tau_{max}=(0.82+0.9\frac{d_B}{l_B})\left(1.6+\frac{0.7c}{d_B}+20\rho_{SV}\right)f_{ct}$	The empirical formula was proposed for confined concrete.
Tang and Cheng [12]	by simple regression, $\tau_{max}=8.9824e^{0.0193f_c'}$ by multiple regression, $\tau_{max}=0.384702f_c'-1.73018d_B-7.40323\frac{c}{d_B}+65.90284$	The formula was proposed for confined concrete. Both pullout and splitting failures exhibited on the used specimens

τ_{max}= Maximum bond stress, d_B= diameter of pulled reinforcement, l_B=bonded length in pullout specimen, c =concrete cover to pulled steel, c/d_B= cover to diameter of pulled reinforcement ratio, d_s= diameter of confining reinforcement, f_c'= compressive strength of concrete, f_{ct}= tensile strength of concrete, f_y= yield strength of reinforcement, ρ_{SV} = stirrup ratio

Table 1: Maximum bond stress equation from different literatures and their criteria.

DESCRIPTION OF REFERENCE SPECIMENS

Three reference specimens from Deng et al. [21] have been selected to validate the proposed finite element modeling strategy with the experimental data. These specimens contain both plain concrete and engineered cementitious composite. Another specimen from Tang and Cheng [12] has been selected to check the performance of the proposed FEM strategy of concrete with confinement. The testing procedure for all reference specimens was almost the same. A universal testing machine provided the pullout load at a specific displacement-controlled rate. Schematic diagrams of the reference specimens are shown in Fig. 1(a)-(b). In the reference experimental program, Eqns. (1)-(2) were used to calculate the bond stress and slip of bonded concrete and reinforcement. The material properties and dimensions of the selected specimens are shown in Tab. 2.

$$\tau=\frac{F}{\pi d l_a} \tag{1}$$

$$s=\frac{s_l+s_f}{2} \tag{2}$$

where, τ is the bond stress, s is the slip, F is the applied load, d is the bar diameter, l_a is the bonded length, s_l and s_f are the slips at the loaded end and the free end, respectively.

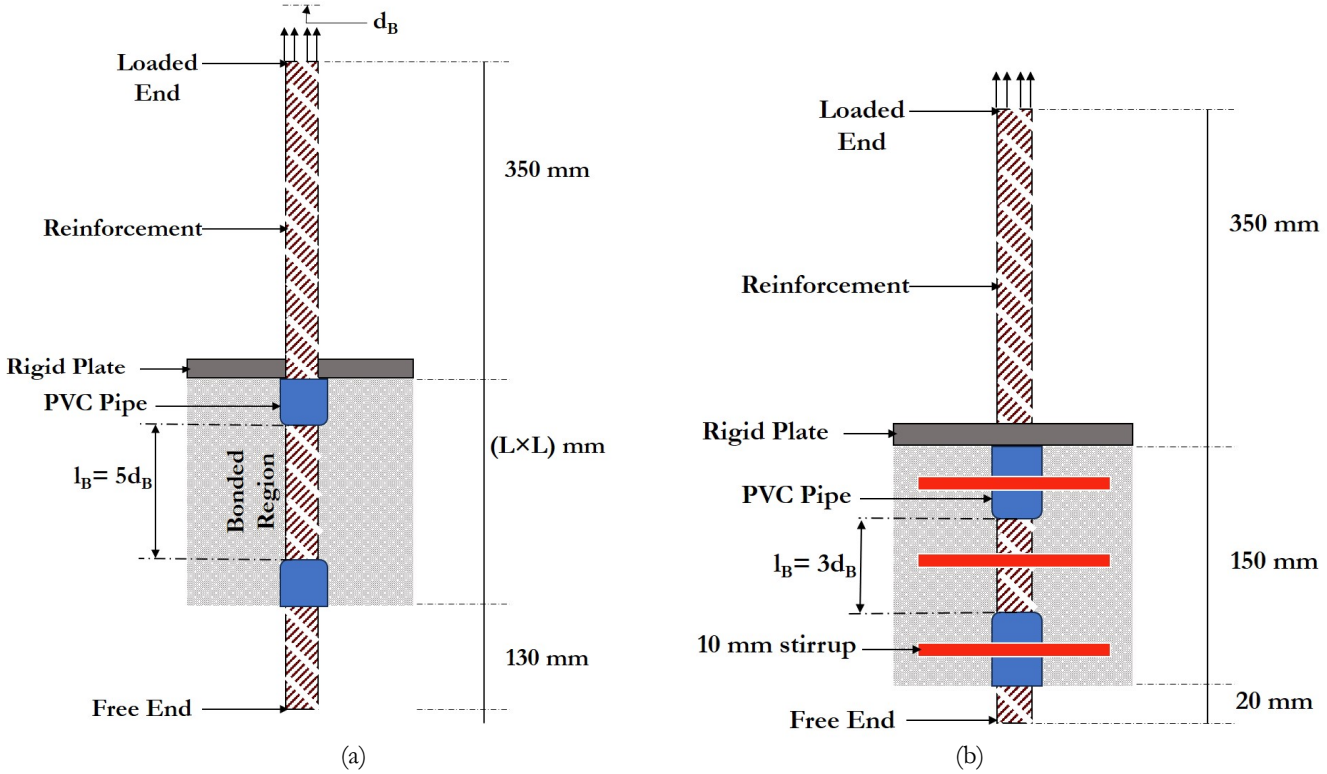

Figure 1: Schematic diagram of reference specimens (a) E1R16, C1R20, E1R16-60 [21] (b) C20#8 [12] (the variable L and d_B can be found in Tab. 2).

References	Specimen	Section size (mm×mm)	d_B(mm)	l_B (mm)	c (mm)	$\frac{c}{d_B}$	d_S (mm)	f'_c (MPa)	f'_y (MPa)
Deng et al. [21]	E1R16	150×150	16	80	67	4.19	-	57.2	471
	C1R20	150×150	20	100	65	3.25	-	50.9	412
	E1R16-60	60×60	16	80	22	1.38	-	57.2	471
Tang and Cheng [12]	C20#8	150×150	25	75	62.5	2.5	10	20.2	471

d_B= diameter of pulled reinforcement, l_B=bonded length in pullout specimen, c=concrete cover to pulled steel, c/d_B= cover to diameter of pulled reinforcement ratio, d_S= diameter of confining reinforcement, f_c'= compressive strength of concrete, f_y= yield strength of reinforcement.

Table 2: Properties of reference specimens.

FINITE ELEMENT MODELLING STRATEGY

A modelling strategy has been developed from scratch to simulate the pullout test of reference specimens in ABAQUS, which is shown by a flowchart in Fig. 2. The definition of concrete-reinforcement interaction is the most crucial factor in bond-slip modelling. Therefore, maximum bond stress must first be predicted for all reference specimens, as all damage initiation and stiffness coefficient parameters depend upon it. At first, the cover-to-diameter ratio (c/d_B) of the reference specimen was considered, and a prediction was made based on the study of Deng et al. [21]. The study found that specimens with a cover-to-diameter ratio of less than or equal to 3.41 exhibited a splitting or splitting-pullout failure pattern. In contrast, those with a cover-to-diameter ratio greater than 3.41 showed a pullout failure pattern. This criterion has been used to predict the failure pattern of the reference specimens.

A literature survey, focusing failure pattern, was conducted to select prediction models to compute the maximum bond stress. Although several previous studies developed empirical formulas for predicting maximum bond stress, the scope of all studies was not the same. Therefore, equations were carefully selected based on the limitations mentioned by the authors in their respective studies. For instance, if a study used pullout failure as the dominant failure type for generating a formula, the proposed equation was used to calculate the maximum bond stress for specimens predicted with pullout failure earlier. Similarly, if both failure patterns were exhibited in the author's used specimens to generate an equation, the equation was used in the specimen with both types of failure patterns. The maximum bond stress of the reference specimen with confinement has been calculated using literatures that considered confinement to generate an empirical formula. An outline of the developed FE models, including considered analytical models for maximum bond stress, are presented in Tab. 3.

The stiffness parameters of the bond-slip behaviour of reinforcement and concrete were calculated using the traction separation law, in which the maximum bond stress calculated by empirical equation was considered as traction. In contrast, the damage initiation parameters were assumed based on the calculated maximum bond stress. Details of constituent material modelling, and other aspects are discussed below:

Model No	References	Specimen	Predicted failure mode	Adopted literatures for bond-slip model
1	Deng et al. [21]	E1R16	Pullout	MC2010-PF [2], Sturm and Visintin [3], Esfahani and Rangan [4], Harajli et al. [5], Huang et al. [6]
2		C1R20	Splitting or Splitting-Pullout	MC2010-SF [2], Sturm and Visintin [3], Harajli et al. [5], Oragun et al. [7], Hadi [8]
3		E1R16-60	Splitting or Splitting-Pullout	MC2010-SF [2], Sturm and Visintin [3], Esfahani and Rangan [4], Harajli et al. [5], Huang et al. [6], Oragun et al. [7], Hadi [8]
4	Tang and Cheng [12]	C20#8	Splitting or Splitting-Pullout	MC2010-SF-C [2], Soroushian and Choi [9], Aslani and Samali [10], Xu [11], Tang and Cheng [12] by simple regression, Tang and Cheng [12] by multiple regression

Table 3: Summary of adopted numerical modeling strategy on reference specimens.

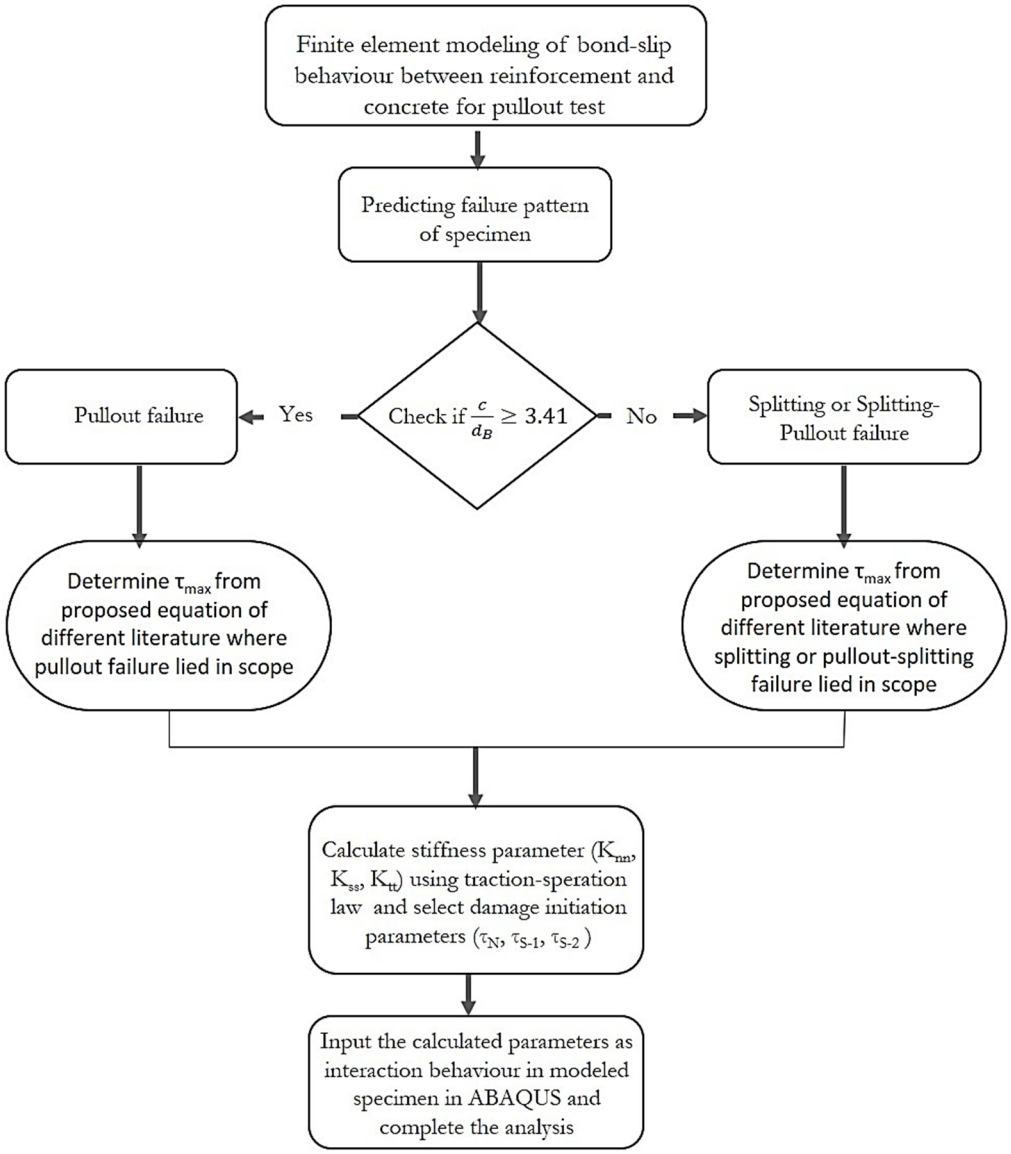

Figure 2: Flowchart of finite element strategy of bond-slip modeling.

Concrete damage plasticity model

As concrete undergoes damages and cracks in the pullout test, the concrete damage plasticity (CDP) model has been selected to capture concrete's nonlinearity, inelastic deformation and shear behaviour. Beliaev et al. [15] found that concrete with an elastic-plastic damage model showed more accurate bond-slip behaviour under the pullout test. An elastoplastic damage model was first proposed by Lubliner et al. [22] for concrete material properties. However, this model showed instability in the softened sections where the material experienced damage and strength reduction. Later, Fenves and Lee [23-25] modified the yield surface initially put forward by Lubiner et al. [22] and proposed a double scalar Concrete-Damaged Plasticity (CDP) model that can capture the complex behaviour of concrete under different loading conditions. The plasticity parameters of concrete have been used with reasonable literature study, as shown in Tab. 4. Compressive and tensile damage variables are used according to GB 50010-2010 [26] and Shao et al. [27]. The constitutive curve of the used CDP model is shown in Fig. 3, which was developed by Shao et al. [27]. The equations mentioned in Shao et al. [27] have been used to calculate the compression and tension curve parameters, as shown in Tab. 5. The compression stress-strain has been assumed to be linear up to 40% of the ultimate compressive strength of concrete.

Parameters	Corresponding values and reference	Selected value
Dilatation Angle	30-35° [28]	31°
Flow potential eccentricity, ε	0.1[31]	0.1
The ratio of biaxial and uniaxial compressive strength, σ_{b0}/σ_{c0}	1.16 [29]	1.16
K_c	0.667 [29]	0.667
viscosity coefficient, μ	0.01-0.0001 [30]	0.0001

Table 4: The parameters used in the CDP model.

Parameters	Equation
Strain for peak compression strength, $\varepsilon_{c,r}$	$\varepsilon_{c,r}=(700+172\sqrt{f_c})\times10^{-6}$
Strain for peak tension strength, $\varepsilon_{t,r}$	$\varepsilon_{t,r}=f_{t,r}^{0.54}\times65\times10^{-6}$
Descending parameters of compression curve, α_c	$\alpha_c=0.157f_c^{0.785}-0.905$
Descending parameters of compression curve, α_t	$\alpha_t=0.312f_{t,r}^2$

Table 5: Used equation for developing parameter for CDP model [26,27].

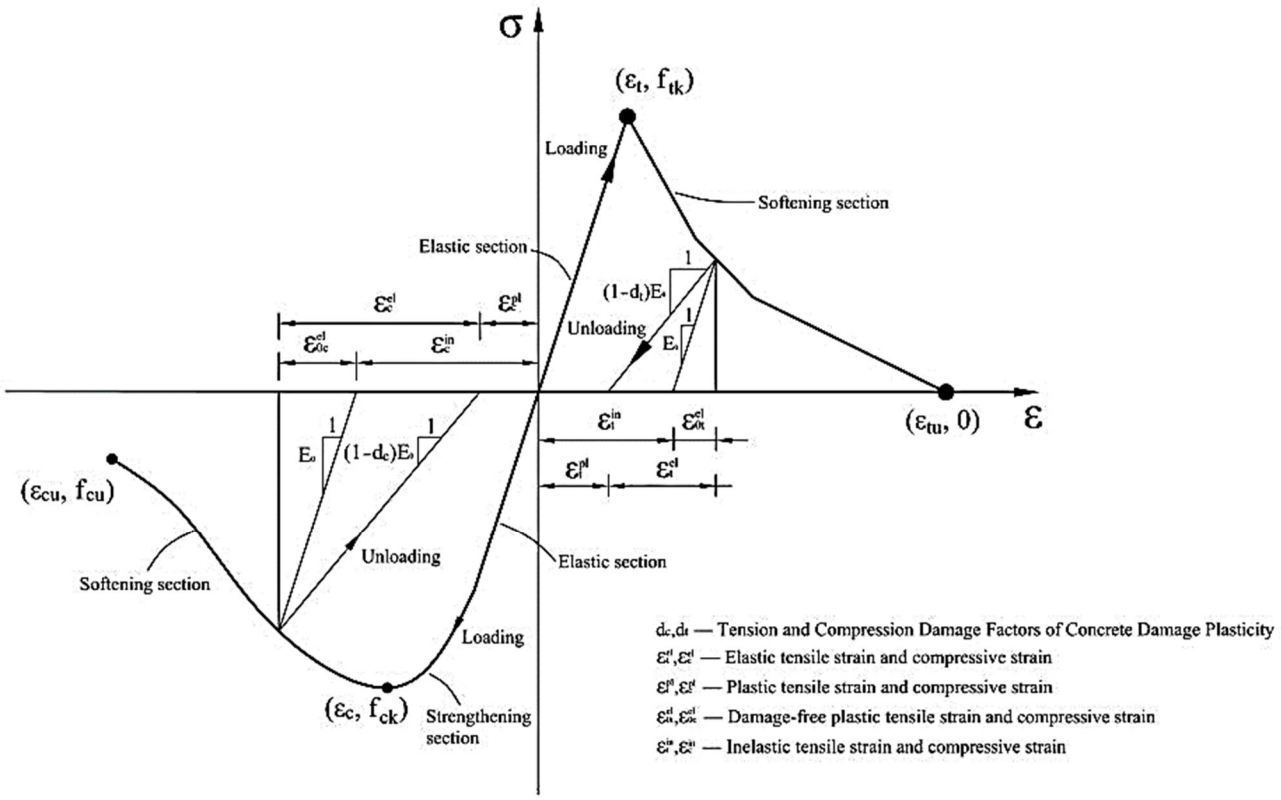

Figure 3: Constitutive curve of the concrete-damaged plasticity model [27].

Eqns. (3)-(6) are used to calculate the plastic compressive and tensile strains of concrete, according to Niu et al. [32].

$$\varepsilon_c^{pl}=\varepsilon_c-\frac{\sigma_c}{(1-d_c)E} \quad (3)$$

$$\varepsilon_{c0}^{pl}=\varepsilon_c-\frac{\sigma_c}{E} \quad (4)$$

$$\varepsilon_t^{pl}=\varepsilon_t-\frac{\sigma_t}{(1-d_t)E} \quad (5)$$

$$\varepsilon_{t0}^{pl}=\varepsilon_t-\frac{\sigma_t}{E} \quad (6)$$

where d is the damage parameter, and σ and ε are the stress and strain of concrete, respectively. The superscripts el and pl refer to elastic and plastic components, respectively, while the subscripts c and t represent compressive and tensile states. The parameter "0" signifies no damage considered.

The compression and tension curve used for this study to model concrete is shown in Fig. 4. The damage parameters have been calculated based on the damage model provided by Sidorroff [33] as per Eqn. 7.

$$d=1-\sqrt{\frac{\sigma}{\varepsilon E}} \quad (7)$$

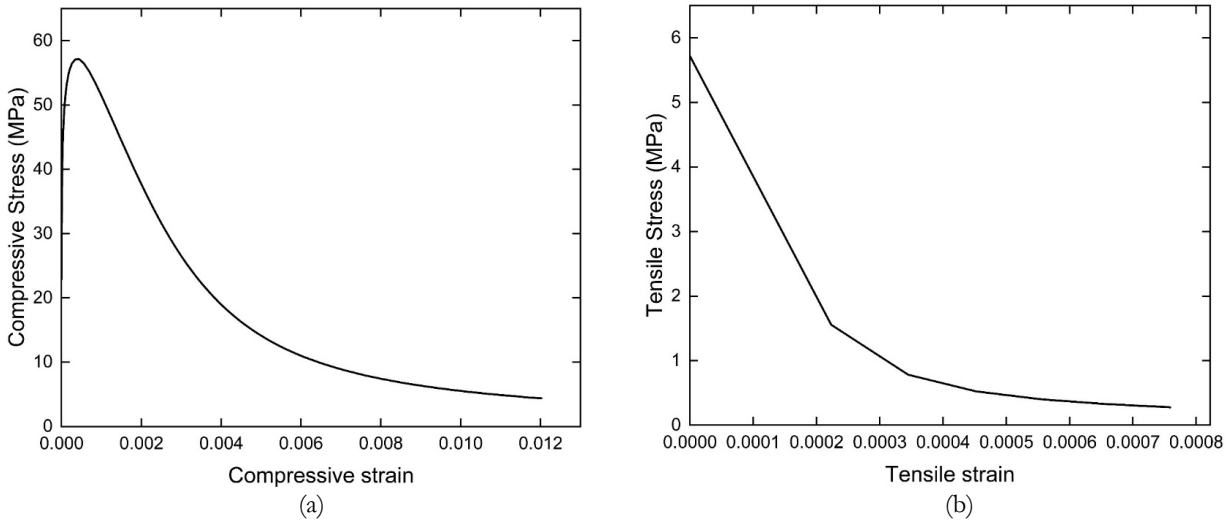

Figure 4: Stress–strain relationship of the concrete-damaged plastic model: (a) compressive stress-strain curve; and (b) tensile stress-strain curve.

Details of modeling

The finite element model was created by generating two parts for the concrete cube and reinforcement. Three-dimensional deformable solid parts have been generated for concrete and reinforcement, and their dimensions are assigned based on Tab. 2. A cylindrical hole was created through the center of the concrete cube with the exact diameter of the reinforcement to ensure interaction between the bonded region of concrete and reinforcement. The rebar was then placed into this hole.

In the experiment conducted by Deng et al. [21], PVC pipe was used at the unbonded region to control the embedded length of reinforcement. However, since PVC material properties were unavailable for this study, PVC pipe has not been used in the unbonded region.

The assignment of holes with different thicknesses may result in the assignment of complex element types. For instance, in this study, the thickness of different hole sizes led to the assignment of an element type of "tet" or "wedge" shape, which is unsuitable for the desired output. Therefore, the hole size has been kept uniform throughout the concrete. However, no

interaction between the concrete and reinforcement has been assigned at the unbonded region. An eight-node linear brick element with reduced integration (C3D8R) has been used as an element type for both the concrete and reinforcement.
The transverse reinforcement has been generated using a three-dimensional deformable wire part for the reference specimen of Tang and Cheng [12]. The truss-type section has been assigned in transverse reinforcement, and its cross-section has been assigned according to Tab. 2. Once the concrete damage plasticity material properties have been assigned to the concrete section, the material property of reinforcement has been defined using yield stress, ultimate stress, and the corresponding strain mentioned in the references [12,21]. Young's modulus and Poisson's ratios were considered 210 GPa and 0.3 for steel rebar, respectively. Finally, the defined material property was assigned to the longitudinal and transverse reinforcement sections.

Loading and boundary conditions

The boundary condition has been resembled according to experimental work [12,21]. In the experiment, the concrete face near the loading end of the reinforcement was fixed by the rigid plate of the loading device [12,21]. Therefore, an encastre boundary condition has been applied on the top face of concrete by which all degrees of freedom (translations and rotations) are constrained to be zero. A reference point has been created above the surface of the loading end of the rebar. A kinematic coupling constraint has been assigned to this reference point, which works as the rebar's control point and loading surface (see Fig. 10). Therefore, all degrees of freedom of the loading surface of the rebar have been constrained at the reference point. The loading end of the rebar was pulled by universal testing machine at a constant displacement rate in the reference experiment [12,21]. Therefore, a displacement of 15 mm has been applied to the reference point. The boundary condition of the whole model is shown in Fig. 5.

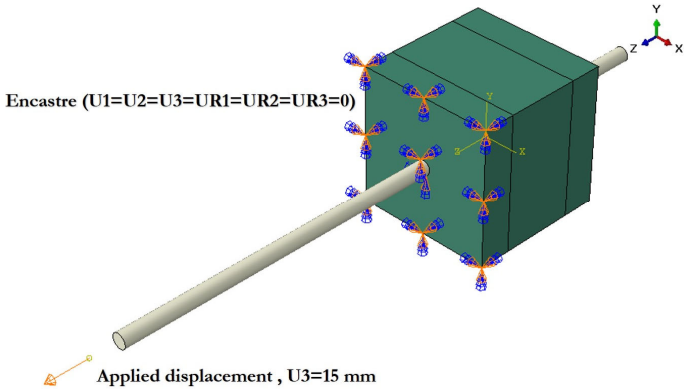

Figure 5: Load and boundary condition of reference specimen E1R16 [21].

Interaction between reinforcement and concrete

In order to transfer load between the bonded region of reinforcement and concrete, a contact model needs to be defined. Two contact models are available in ABAQUS: node-to-node and surface-to-surface contact models. The surface-to-surface contact model imposes contact criteria on average across regions of the "master" and "slave" surfaces [34,35]. However, when a sharp object, such as a bullet or pin, hits a flat surface, it is best to use the node-to-surface contact model, where the point of contact is between the surface and the object [36]. In the pullout test, where the surface of reinforcement moves relative to the surface of concrete, the surface-to-surface contact model is the relatively good contact model that reflects the actual bond-slip behaviour, and this model has been used in other studies [37,38]. Therefore, the surface-to-surface contact model has been implemented in this study.
Normal, tangential, cohesive, and damage behaviour have been specified for successfully formulating the surface-to-surface contact model. "Hard" contact has been defined in normal behaviour, as reinforcement and concrete surfaces are pressed against each other. It enforces infinite stiffness, meaning the surfaces cannot penetrate each other. However, separation is allowed after contact.
Coulomb's law of friction has been used to define the tangential behaviour of the reinforcement-concrete interface. Idun & Darwin [39] observed a friction coefficient of around 0.5 between steel reinforcement and concrete. Therefore, a friction coefficient of 0.5 has been used to define the tangential behaviour to reflect the roughness between the reinforcement and concrete surface.

Cohesive behaviour has been assigned to simulate the bond-slip interaction property between concrete and reinforcement. The bond-slip model proposed by Eligehausen et al. [40], also prescribed by Model Code 2010 [2], has been used in this study, as shown in Fig. 6. It shows three phases:

- An ascending part up to a maximum stress
- A plateau for confined concrete
- A descending part that refers to the reduction of bond resistance due to the shearing off of concrete corbels between the ribs

The parameters of bond-slip model are calculated using the traction separation law in ABAQUS, as shown in Fig. 7. The traction-separation curve has a linear ascending branch until the peak traction of t°_{n} (t°_{s}, t°_{t}) and separation of δ°_{n} (δ°_{s}, δ°_{t}). After reaching this point, the damage initiation and the descending branch of the curve continue until the traction reaches zero.

Eqn. (8) expresses the linear-elastic traction-separation law for the uncoupled stiffness option. As insufficient data is available to determine all the stiffness coefficients of the coupled option, the uncoupled option has been chosen.

$$\begin{Bmatrix} t_n \\ t_s \\ t_t \end{Bmatrix} = \begin{bmatrix} K_{nn} & 0 & 0 \\ 0 & K_{ss} & 0 \\ 0 & 0 & K_{tt} \end{bmatrix} \begin{Bmatrix} \delta_n \\ \delta_s \\ \delta_t \end{Bmatrix} \tag{8}$$

where t_n, t_s, and t_t represent normal traction and shear traction in two directions, respectively. δ_n, δ_s, and δ_t represent separations or displacements in normal and two shear directions. K_{nn}, K_{ss}, and K_{tt} represents stiffness coefficients in normal and two shear directions, respectively.

K_{ss} and K_{tt} have been obtained by the bond-slip relationship shown in Fig. 6 using Eqn. (9). According to Keuser et al. [43], K_{nn} could be determined by Eqn. (10).

$$K_{ss} = K_{tt} = \frac{\tau_{max}}{s_1} \tag{9}$$

$$K_{nn} = 100K_{ss} = 100K_{tt} \tag{10}$$

In this study, actual bond-slip behaviour has been approximated by overlapping traction separation law, as shown in Fig. 8. Therefore, the stiffness coefficient in the shear direction (K_{ss}, K_{tt}) could be obtained from maximum bond stress (τ_{max}) and slip at maximum bond stress (s_1) (see Fig. 8). A limitation is that, unlike traction separation law, true bond-slip relation has a transition phase from damage initiation to peak. However, the traction separation curve is linear up to peak bond stress where the damage initiation started. Luna Molina [19] used maximum bond stress and corresponding slip to define damage initiation parameters, which resulted in stiffness changes with an accurate approximation of maximum bond stress. This study defines damage parameters by the maximum nominal stress criterion (the stress at which degradation starts). The accuracy of maximum bond stress and stiffness has been emphasized the most in this study. Therefore, maximum bond stress calculated by equations of different literature has been used as damage initiation parameters. Afterwards, the damage evolution criterion has been defined. It is the process by which cohesive stiffness is degraded after meeting the damage initiation criterion. Displacement-based damage evolution, where total or plastic displacement represents the extent of damage over time as the object continues to degrade, has been adopted in this study. This approach is commonly referred to as displacement at failure [34].

Model code 2010 [2] suggested using a clear distance between ribs as s_3 (see Fig. 6), which is a slip at the failure of the pullout test. In this study, the clear distance between ribs has been used as plastic displacement in damage evolution for reference specimens, predicted with pullout, splitting-pullout, and splitting with confinement failure earlier. However, a plastic displacement of 1.0 mm is assumed to be plastic displacement for reference specimens with splitting failure, which typically has less softening region than other failure types (see Fig. 6). For the calculation of stiffness coefficients using Eqn. (9), the slip at damage initiation (s_1) value has been selected through a reasonable literature study shown in Fig. 9. The slip at damage initiation value varied from literature to literature, directly affecting the bond-slip curve's stiffness. The slip value at damage initiation (s_1) in the 0.1-0.2 mm range has dominated the literature study. Therefore, the slip at damage initiation has been used as 0.1 mm for reference specimens that predicted pullout, splitting-pullout and reference specimens with confinement. For reference specimens with splitting failure, slip at damage initiation of 0.15 mm has been used except for

Harajli et al. [5]. The details of calculating these stiffness coefficients and damage initiation parameters are shown in Tab. 6. Moreover, the softening region of the bond-slip relationship has been considered linear in the damage evolution segment in ABAQUS.The calculated parameters have been assigned to cohesive contact interaction property, and surface-to-surface contact has been assigned to the bonded region of reinforcement and concrete (see Fig. 10). For reference specimens of Tang and Cheng [12], the transverse reinforcements have been embedded in concrete cubes without considering any cohesive interaction to avoid complexity.

Finite element mesh

In this study, a mesh size of 10 mm is used for both concrete cube and reinforcement. In the concrete cube, 4800 hexagonal elements have been created. In reinforcement, a total of 324 hexagonal elements have been created. The finite element mesh of the reference specimen C1R20 [21] is shown in Fig. 11.

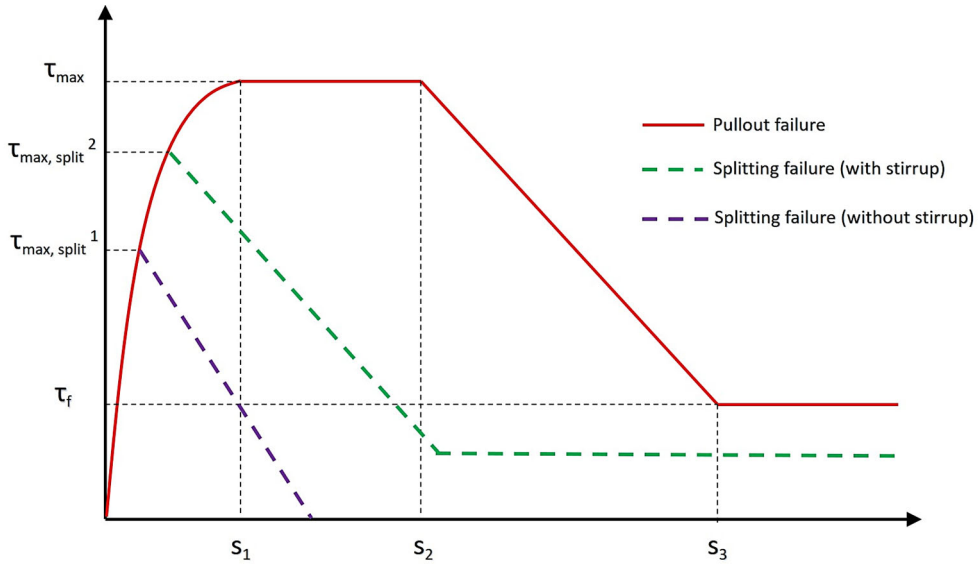

Figure 6: Analytical bond stress-slip relationship for monotonic loading [2].

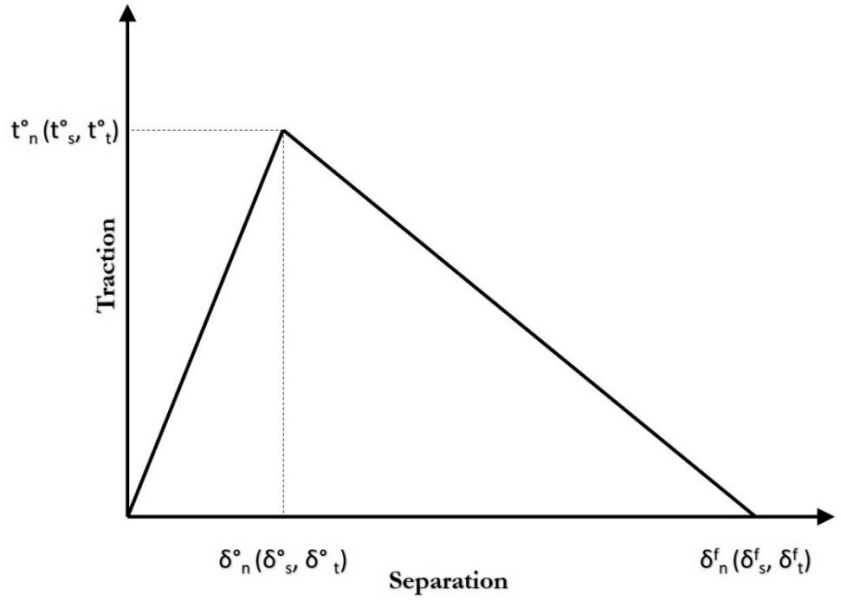

Figure 7: Traction separation law available in ABAQUS [34].

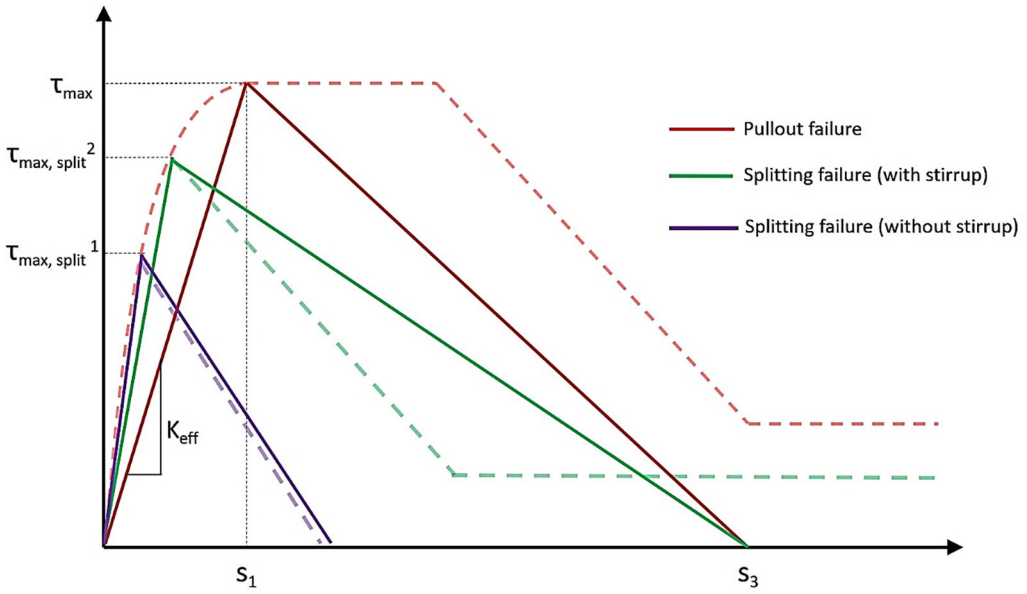

Figure 8: Approximation of bond-slip behavior (dotted line) using traction separation law (solid line).

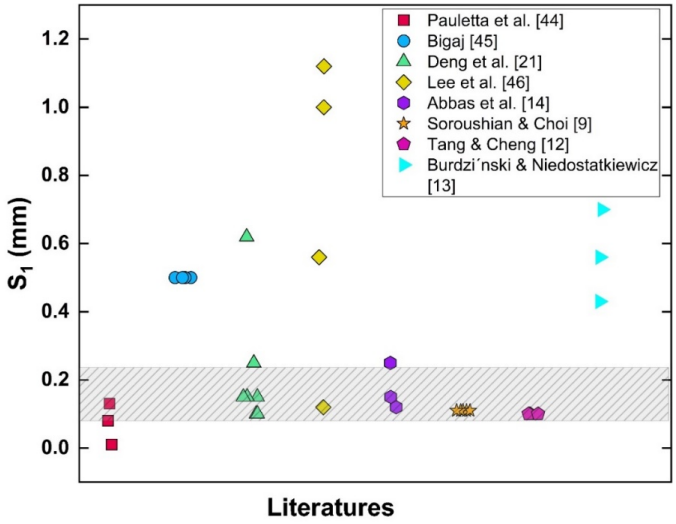

Figure 9: Literature study of slip at damage initiation (S_1) from different literature.

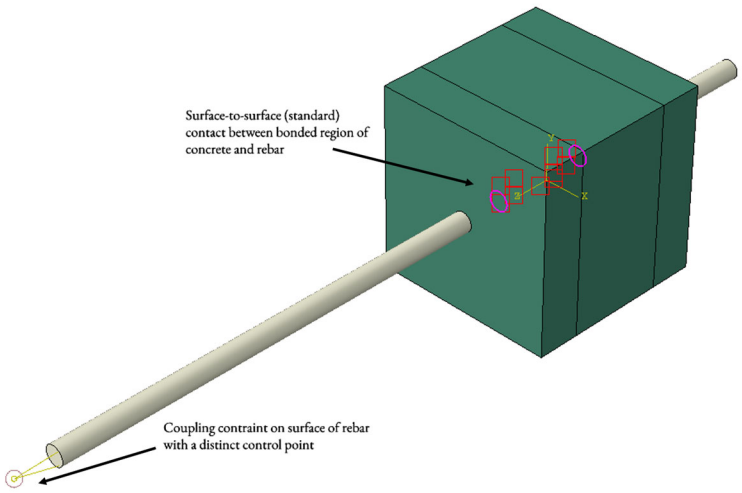

Figure 10: Constraint and interaction of reference specimen E1R16 [21].

Reference specimen	Observed failure mode	Adopted models	τ_{max} (MPa)	Stiffness parameters (MPa/mm)		Damage initiation parameters		
				K_{nn}	$K_{ss}=K_{tt}$	$\tau_n= \tau_{s-1}= \tau_{s-2}$ (MPa)	S_1 (mm)	P_d (mm)
E1R16	Pullout	MC2010-PF [2]	18.908	18908	189.08	18.908	0.1	26
		Sturm and Visintin [3]	17.538	17538	175.38	17.538	0.1	26
		Esfahani and Rangan [4]	21.223	21223	212.23	21.223	0.1	26
		Harajli et al. [5]	19.437	19437	194.37	19.437	0.1	26
		Huang et al. [6]	25.74	25740	257.4	25.74	0.1	26
C1R20	Splitting	MC2010-SF [2]	8.841	58.94	58.94	8.841	0.15	1
		Sturm and Visintin [3]	15.423	10282	102.82	15.423	0.15	1
		Harajli et al. [5]	18.335	7334	73.34	18.335	0.25	1
		Oragun et al. [7]	12.412	8274.66	82.746	12.412	0.15	1
		Hadi [8]	8.58	5720	57.2	8.58	0.15	1
E1R16-60	Pullout + Splitting	MC2010-SF [2]	9.103	9103	91.03	9.103	0.1	26
		Sturm and Visintin [3]	12.904	12904	129.04	12.904	0.1	26
		Esfahani and Rangan [4]	11.962	11962	119.62	11.962	0.1	26
		Harajli et al. [5]	19.437	19437	194.37	19.437	0.1	26
		Huang et al. [6]	25.74	25740	257.4	25.74	0.1	26
		Oragun et al. [7]	9.625	9625	96.25	9.625	0.1	26
		Hadi [8]	9.34	9340	93.4	9.34	0.1	26
C20#8	Splitting	MC2010-SF-C [2]	8.02	8020	80.2	8.02	0.1	25
		Soroushian and Choi [9]	11.283	11283	112.83	11.283	0.1	25
		Aslani and Samali [10]	12.901	12901	129.01	12.901	0.1	25
		Xu [11]	11.747	11747	117.47	11.747	0.1	25
		Tang and Cheng [12] by simple regression	13.265	13265	132.65	13.265	0.1	25
		Tang and Cheng [12] by multiple regression	11.911	11911	119.11	11.911	0.1	25

τ_n= Maximum nominal stress in normal direction, τ_{s-1}= Maximum nominal stress in shear-1 direction, τ_{s-2} = Maximum nominal stress in shear-2 direction, P_d= Total/Plastic displacement

Table 6: Calculation of stiffness coefficients and damage initiation parameters.

Solution procedure

In the pullout test, concrete crushes locally when reinforcement is pulled in tension. The crushing in concrete initiated stiffness degradation and softening behaviour, which caused convergence issues in the static analysis [34,47]. Therefore, a dynamic implicit-solving strategy has been implemented in this study. However, the simulation solution strategy in the dynamic implicit method still needs to carefully select increment size as small changes in increment could result in skipping important output. Therefore, the maximum and minimum number of increments have been used as 10^4 and 10^{-15}, respectively. The initial increment size has been used as 0.0001. All other options have been kept as default. Nonlinear geometry has been kept on.

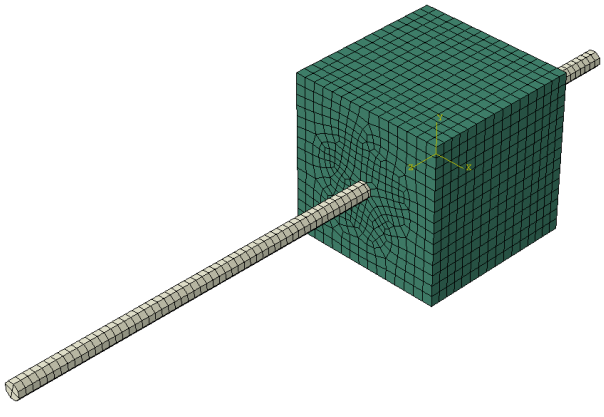

Figure 11: Finite element mesh (10 mm) of reference specimen E1R16 [21].

FINITE ELEMENT RESULT AND ANALYSIS

The proposed finite element modelling strategy has been validated with experimental data from references [12,21] for the bond stress-slip relationship and failure pattern.

Mesh sensitivity analysis

In this study, a mesh sensitivity analysis has been performed on mesh sizes of 10 mm, 20 mm, 30 mm, and 40 mm for reference specimen C1R20. The failure pattern of the experiment and FEM models for reference specimen C1R20 are shown in Fig. 13 (a)-(e). The analysis revealed that 20 mm and 30 mm mesh sizes showed almost mesh-independent results regarding bond stress vs. slip curves, as shown in Fig. 12. Although a mesh size of 40 mm showed a more accurate maximum bond stress relative to the experiment, the failure pattern did not resemble the experiment (see Fig. 13 (a) and 13 (e)). On the contrary, the mesh size of 10 mm has shown more accurate output in terms of failure pattern relative to the experiment, as shown in Fig. 13 (b). It is evident from Fig. 13(b)-(e) that a finer mesh size can lead to a representative concrete damages in the pull out test. Therefore, more refinement of the mesh size would help to capture more accurate damage propagation in concrete, however, it may need more computational time. Therefore, a mesh size of 10 mm or larger may be employed to estimate the specimen strength (i.e., peak stress), as evident in Fig. 12, however a finer mesh is required to analyze the damage propagation with high computational time. Thus, all FEM analyses for all reference specimens were performed with a mesh size of 10 mm to maintain uniformity of this study.

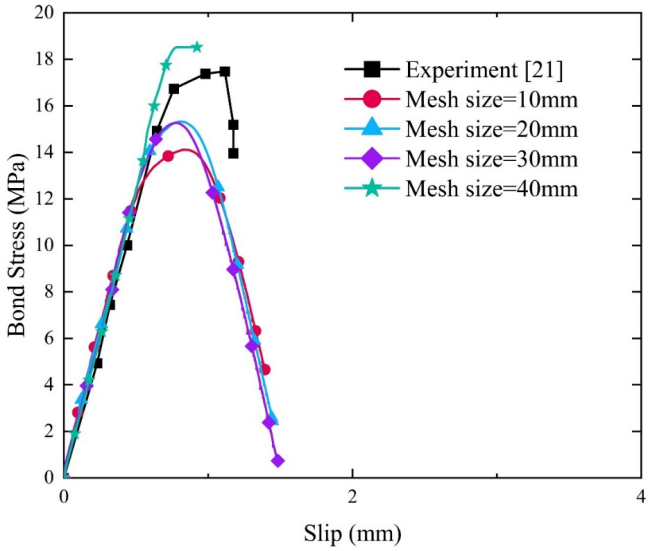

Figure 12: FEM mesh sensitivity analysis.

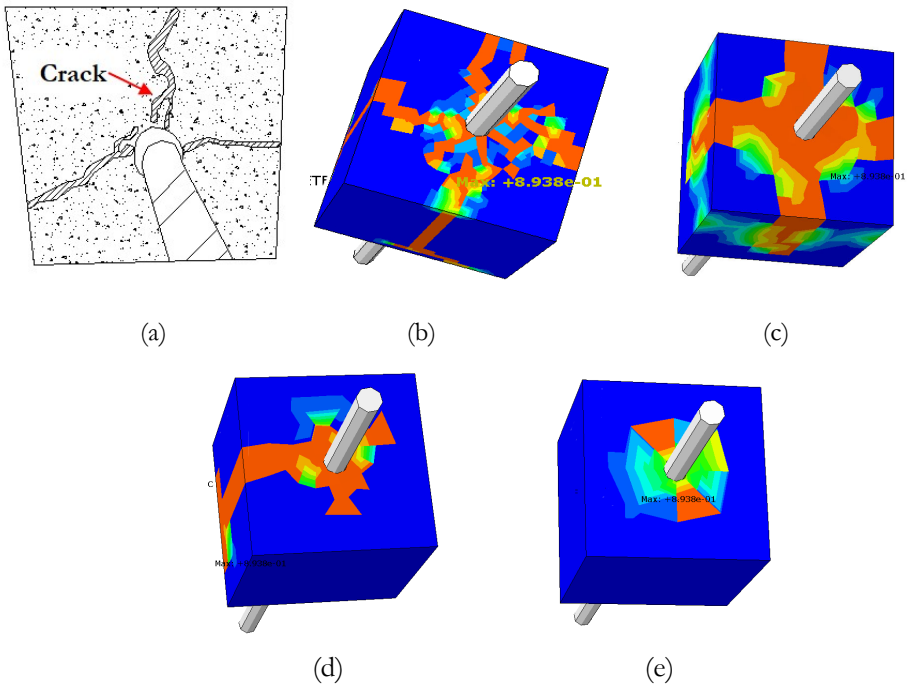

Figure 13: Failure pattern of reference specimen C1R20 [21] (a) Experimental (Schematic), (b) 10 mm mesh, (c) 20 mm mesh (d) 30 mm mesh (e) 40 mm mesh.

Reference specimens expected to have pullout failure

Bond stress-slip behavior

Fig. 14 shows the experimental and finite element bond stress vs. slip behavior of the reference specimen E1R16, whose failure has been predicted as pullout failure. In the finite element analysis, several bond stress-to-slip relationships, i.e., analytical models [2-6], have been considered, as discussed earlier. All the analytical models performed well in predicting the bond stress slip behavior in the elastic regime. The finite element bond stress at peak resistance showed 0.6 ~ 3.3 MPa deviation when compared to the experimental result. The FEM developed using the analytical model by Strum and Visintin [3] showed the most accurate prediction, i.e., 96.7% accuracy in predicting maximum bond stress when compared to that of the experimental result. However, much deviation has been found in the post-peak regime, as evidenced by Fig. 14.

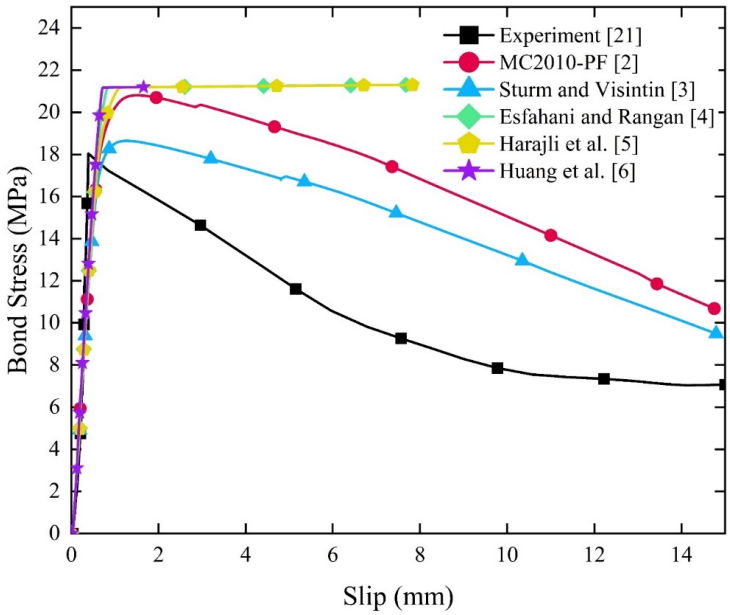

Figure 14: Bond Stress Vs Slip for reference specimen E1R16 [21].

The FEM developed using analytical models by Model Code [2] and Strum and Visintin [3] could resemble the post-peak bond stress degradation phenomenon of the reference test specimen. Nevertheless, the FEM developed using analytical models by Esfahani and Rangan [4], Harajli et al. [5], and Huang et al. [6] did not show the stress degradation phenomenon that could be attributed to the failure mechanism in the FE analysis which will be discussed in the following subsection.

Failure modes

The reference specimen E1R16 [21] failed at concrete to reinforcement bond in the experiment. In finite element analysis, two different modes of failures, initial splitting followed by pullout and steel yielding have been observed. In FE models developed using Model Code [2] and Strum and Visintin [3], failure was initiated by splitting followed by pullout failure. For instance, the failure mechanism of the FE model developed using the analytical model by Strum and Visintin [3] at peak resistance is illustrated in Fig. 15 (a)-(c). Fig. 15 (a)-(b) shows that the surrounding concrete of the bonded region nearly failed due to tension at peak resistance, as the tension damage factor is very close to unity (d_t =0.89). Meanwhile, the scaler stiffness degradation (SDEG) variable of the bonded concrete region, as shown in Fig. 15 (c), is found to be 0.85 at peak, indicating that the border region of the concrete is still not damaged completely. Therefore, pullout failure has not been stated at the peak resistance. Furthermore, the contact status of the bonded surface has been checked to ensure the failure mechanism was correct. At peak resistance, where a slip of 1.28 mm occurred, both concrete and rebar regions mostly bonded with each other, as shown in Fig. 16. However, at the final loading stage, i.e., a slip of 14.79 mm, the bonded portion of rebar has started to slide over concrete, and some regions have not been in contact with each other, which indicates a partial pullout failure at the end stage. In addition, stresses on pulled reinforcement have been checked to confirm that they do not have steel yielding. Von Mises' stress output is shown in Fig. 17. It is evident that the pulled reinforcement in the FEM, developed using the analytical model by Strum and Visintin [3], has yet to yield as maximum Mises stress (=204 MPa) is less than yield strength (=471 MPa). Therefore, the failure pattern has been initiated by splitting and followed by partial pullout.In other FE models, developed using Esfahani and Rangan [4], Harajli et al. [5], and Huang et al. [6], pulled reinforcement yielded at peak. For instance, Mises' stress of the reinforcement in the FE models, developed using analytical models by Esfahani and Rangan [4], Harajli et al. [5], and Huang et al. [6], has found 491 MPa, 491 MPa, and 474 MPa, respectively, which is greater than the yield stress (=471 MPa) of the reference specimen. It is to be noted that due to the idealization of the tensile behavior of steel, i.e., the bilinear relationship bond stresses did not show any degradation, as mentioned in the earlier subsection.

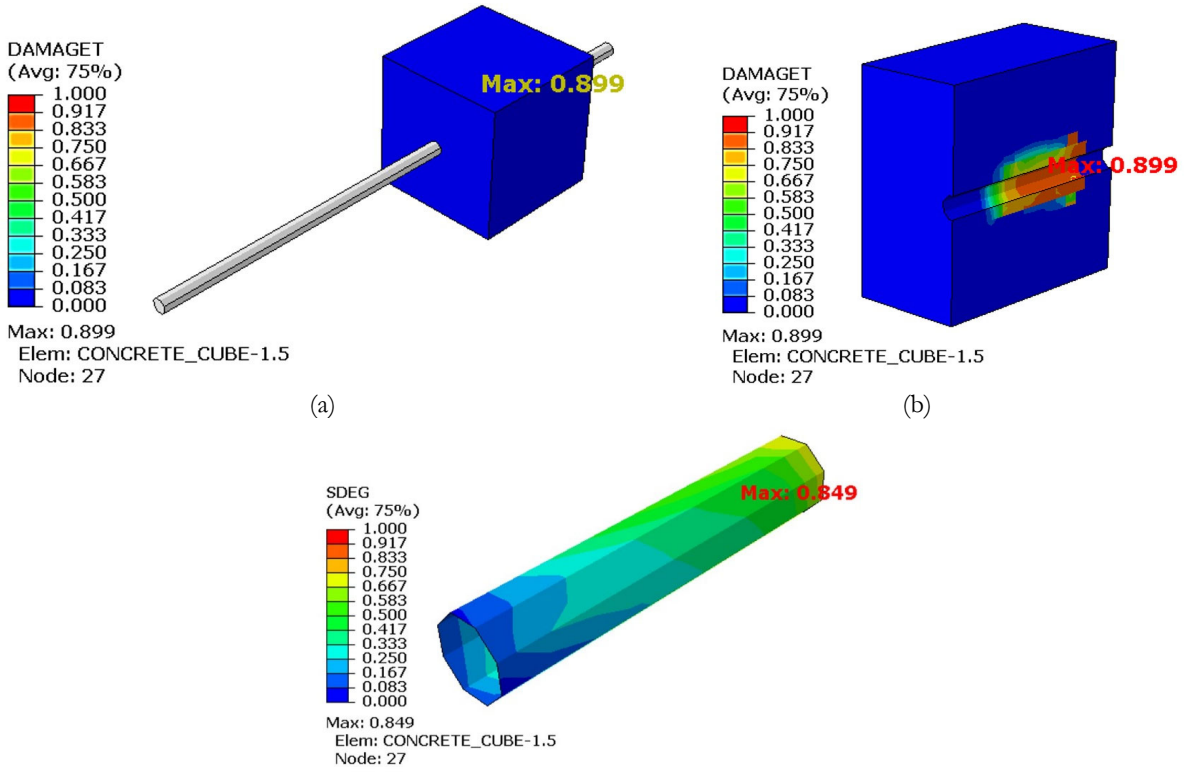

Figure 15: Pullout failure pattern of reference specimen E1R16 [21] (a) experimental (b) DamageT output of the numerical model (c) DamageT output (d) SDEG output of concrete-reinforcement bonded region.

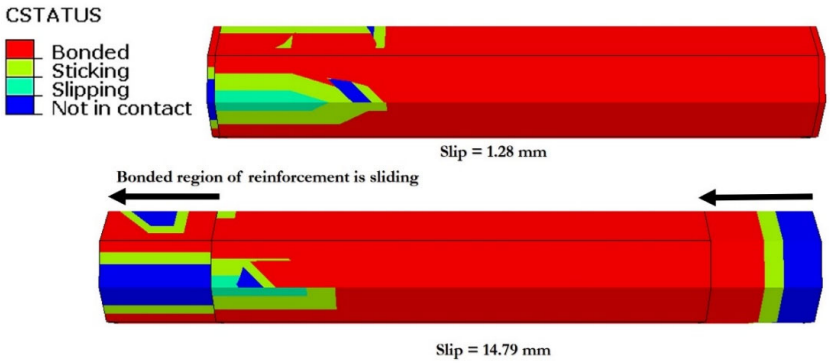

Figure 16: Contact status of bonded region of concrete-reinforcement of reference specimen E1R16.

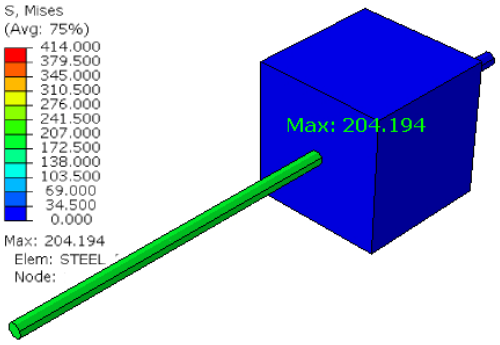

Figure 17: FEM Von Mises Stresses of reference specimen E1R16 [21] using equation of Strum and Visintin.

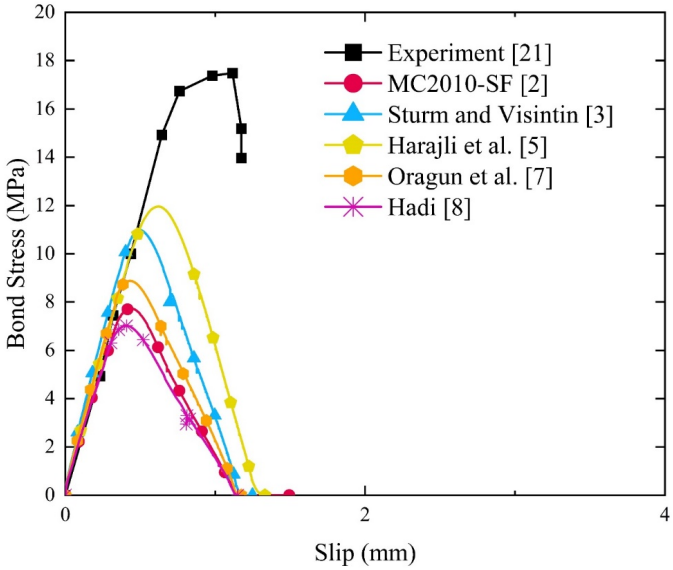

Figure 18: Bond Stress Vs Slip for reference specimen C1R20 [21].

Reference specimens expected to have splitting or splitting-pullout failure

Bond stress-slip behavior

Fig. 18 shows the experimental and finite bond stress vs. slip behavior of the reference specimen C1R20, whose failure has been predicted as splitting or splitting-pullout failure. Suitable analytical models [2, 3, 5, 7, 8] have been considered to determine several bond stress-to-slip relationships for performing finite element analysis. It is evident that the analytical models accurately predicted bond stress to slip behavior in the elastic region. However, the finite element bond stress at the peak showed a 5.52 ~ 10.46 MPa deviation when compared to the experimental result. The FEM developed using the

analytical model by Harajli et al. [5] showed the closest prediction, i.e., 68.4% accuracy in predicting maximum bond stress when compared to that of the experimental result. Therefore, this numerical modeling method has not accurately predicted the maximum bond stress of reference specimens with splitting failure. The probable reason for this underestimation of FEM maximum bond stress will be discussed in the following subsection.

The proposed modeling strategy could not differentiate between splitting and splitting-pullout failure. However, a tiny softening region of the bond-slip curve has been found after running a single analysis. This small softening region indicated that the reference specimen showed only splitting failure. Therefore, running an analysis with a lower plastic deformation value (i.e., 1 mm in this study) would be better and less time-consuming. The rest of the analyses for this reference specimen have been conducted for plastic deformation of 1 mm. However, if a distinct softening region is found, the reference specimen has been predicted with splitting-pullout failure.

Failure modes

The reference specimen C1R20 [21] failed at concrete splitting in the experiment, as shown in Fig. 19 (a). In FE models developed for all analytical models [2, 3, 5, 7, 8], failure has been initiated by splitting followed by pullout failure. For instance, the failure mechanism, at peak resistance, of the FE model developed using the analytical model by Harajli et al. [5] is illustrated in Fig. 19 (b)-(c). Fig. 19 (b) shows the concrete face splits, identical to the experiment shown in Fig. 19 (a). Fig. 19 (b) shows that the surrounding concrete of the bonded region nearly failed due to tension at maximum bond stress, as the tension damage factor is very close to unity (dt =0.89). Meanwhile, the scaler stiffness degradation (SDEG) variable of the bonded concrete region, as shown in Fig. 19 (c), was found to be 0.87 at peak, indicating that the border region of the concrete is still not damaged completely. The contact status of the bonded surface has been checked to ensure the failure mechanism was correct. At peak resistance, where a slip of 0.61 mm occurred, both concrete and rebar regions completely bonded with each other, as shown in Fig. 20. However, at the loading stage after peak, i.e., a slip of 1.26 mm, the bonded portion of rebar has started to slide over concrete, and some regions have not been in contact with each other. At the final loading stage, i.e., a slip of 1.5 mm, the bonded portion of rebar is completely not in contact with concrete, which indicates a complete pullout failure at the end stage. Fig. 21 describes the crack propagation method in reference specimen C1R20, where the SDEG output of cutting half of the specimen is shown. It can be seen that the crack started to propagate radially at the very beginning of pulling out of the rebar. As there was no transverse reinforcement to prevent propagating cracks, some portions of the concrete face started to split at a slip of 0.002 mm. At maximum bond stress, several portions of the concrete face split at a slip of 0.88 mm. This quick crack propagation of reference specimen in finite element analysis may lead to an underestimation of maximum bond stress compared to the experiment.

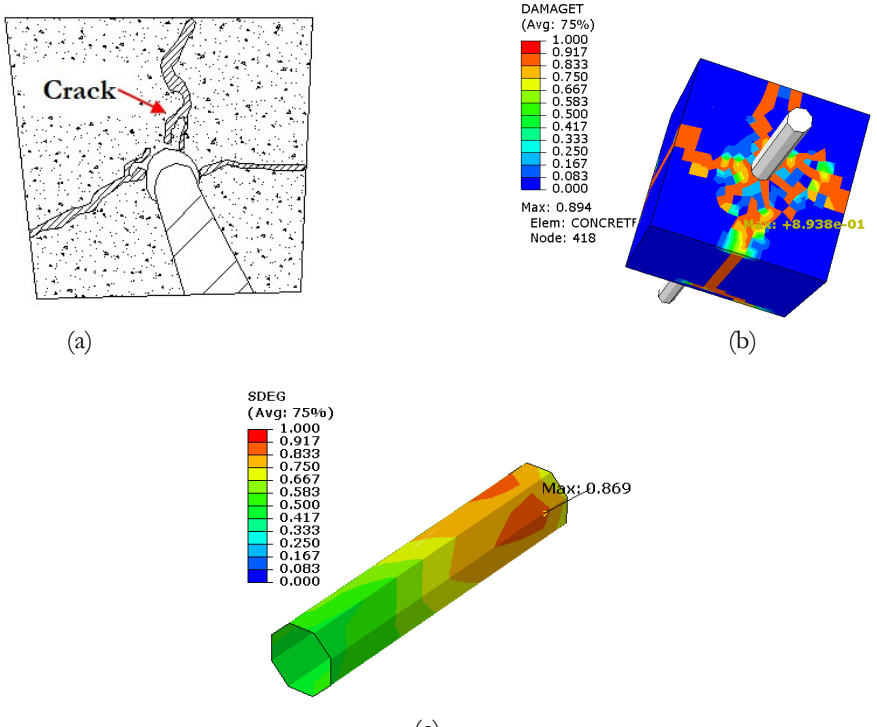

Figure 19: Splitting failure pattern of reference specimen C1R20 [21] (a) experimental (b) damageT output of numerical modeling (c) SDEG output of concrete-reinforcement bonded region.

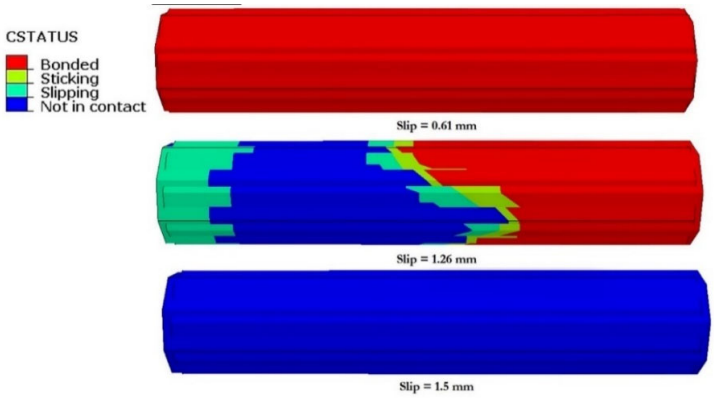

Figure 20: Contact status of bonded region of concrete-reinforcement of reference specimen C1R20.

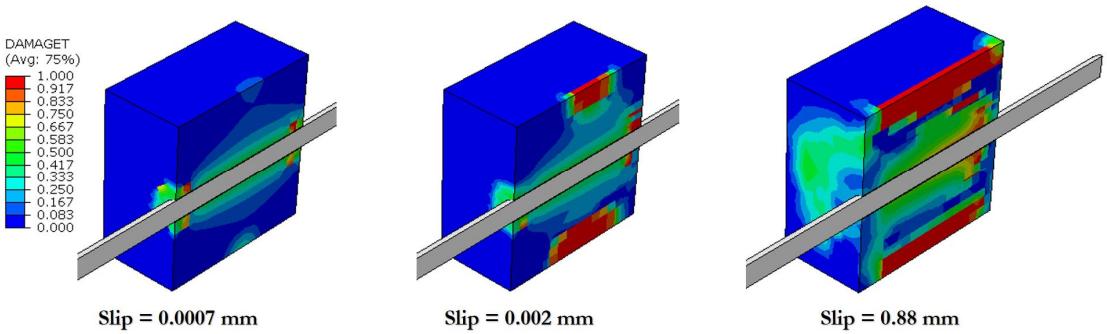

Figure 21: Cracking propagation in reference specimen C1R20.

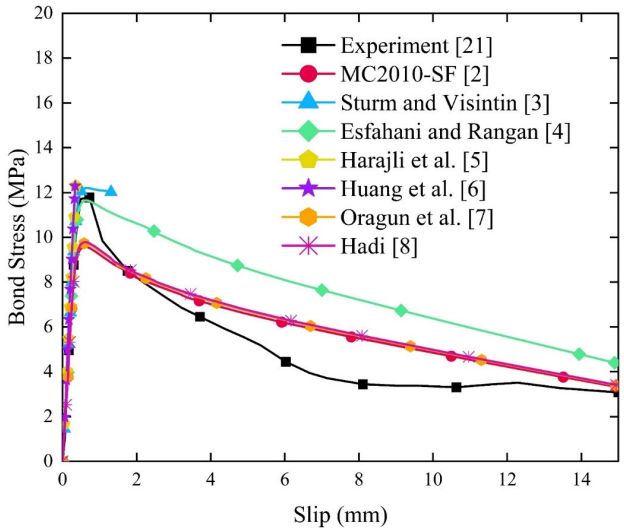

Figure 22: Bond Stress Vs Slip for reference specimen E1R16-60.

Reference specimens expected to have splitting-pullout failure

Bond stress-slip behavior

Fig. 22 shows the experimental and finite element bond stress vs. slip behavior of the reference specimen E1R16-60, whose failure has been predicted as splitting or splitting-pullout failure. Due to having a distinct softening region in the bond-slip curve, the splitting-pullout failure pattern has been confirmed later. Several bond stress-to-slip relationships, i.e., analytical models [2-8], have been considered in the finite element analysis. All the analytical models performed well in predicting the bond stress-to-slip behavior in the elastic regime. The finite element bond stress at peak resistance showed 0.04 ~ 2.11 MPa deviation compared to the experimental result. The FEM developed using the analytical model by Esfahani and Rangan [4]

showed the most accurate prediction, i.e., 99.7% accuracy in predicting maximum bond stress when compared to that of the experimental result. However, much deviation has been found in the post-peak regime, as evidenced by Fig. 22. The FEM developed using analytical models by Harajli et al. [5], and Huang et al. [6] stopped before completion.

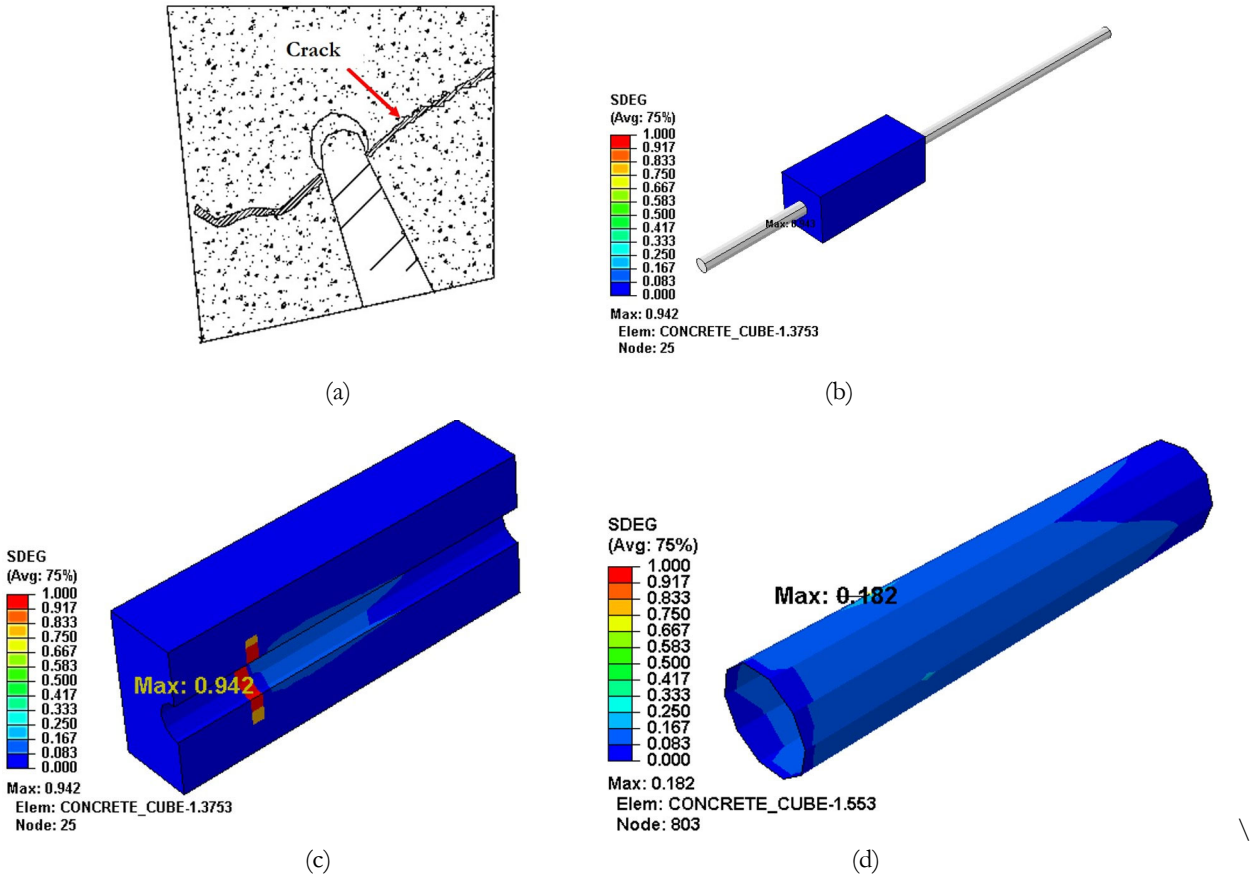

Figure 23: Pullout-Splitting failure pattern of numerical modelling of reference specimen E1R16-60 [21].

Failure modes

The reference specimen E1R16-60 [21] failed at the combination of both splitting and pullout in the experiment, as shown in Fig. 23 (a). Fig. 23 (a) shows the reference specimen E1R16-60 having a distinct split on the face of the concrete. The FE models have not shown any cracks on the concrete face, as shown in Fig. 23 (b). However, Fig. 23 (c) shows a crack propagation through the concrete cover. Unlike the experiment, the propagated crack has not reached the concrete face, which may be why the crack is not showing on the concrete face.

In FE models developed for all analytical models [2-8], failure was initiated by splitting followed by pullout failure. For instance, the failure mechanism, at peak resistance, of the FE model developed using the analytical model by Esfahani and Rangan [4] is illustrated in Fig. 23 (b)-(d). Fig. 23 (b)-(c) shows that the surrounding concrete of the bonded region nearly failed due to tension at peak resistance, as the tension damage factor is very close to unity (dt =0.94). Meanwhile, the scaler stiffness degradation (SDEG) variable of the bonded concrete region, as shown in Fig. 23 (d), was found to be 0.18 at the peak, indicating that the border region of the concrete has just started to degrade. Therefore, pullout failure has not been started at the peak resistance. Furthermore, the contact status of the bonded surface has been checked to ensure the failure mechanism was correct. At peak resistance, where a slip of 0.63 mm occurred, both concrete and rebar regions mostly bonded with each other, as shown in Fig. 24. However, at the final loading stage, i.e., a slip of 15 mm, the bonded portion of rebar has started to slide over concrete, and some regions have not been in contact with each other, which indicates a partial pullout failure at the end stage.

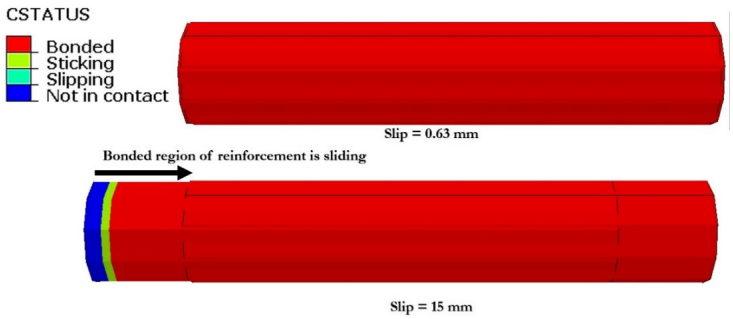

Figure 24: Contact status of bonded region of concrete-reinforcement of reference specimen E1R16-60 [21].

Reference specimen with confinement

Bond stress-slip behavior

Fig. 25 shows the experimental and finite element bond stress vs. slip behavior of the reference specimen C20#8 [12], whose failure has been predicted as splitting or splitting-pullout failure. In the finite element analysis, several bond stress-to-slip relationships, i.e., analytical models [2, 9-12], have been considered, as discussed earlier. All the analytical models performed well to predict the bond stress slip behavior in the elastic regime. The finite element bond stress at peak resistance showed 0.3 ~ 2.4 MPa deviation when compared to the experimental result. The FEM developed using the analytical model by Tang and Cheng [12] by multiple regression showed the most accurate prediction, i.e., 97.9% accuracy in predicting maximum bond stress when compared to that of the experimental result.

The FEM has not shown any plateau region (see Fig. 25) because the used traction separation law to approximate bond-slip behavior has no plateau region (see Fig. 8). Due to this reason, slip at maximum bond stress has been found to be more conservative than that of the experiment.

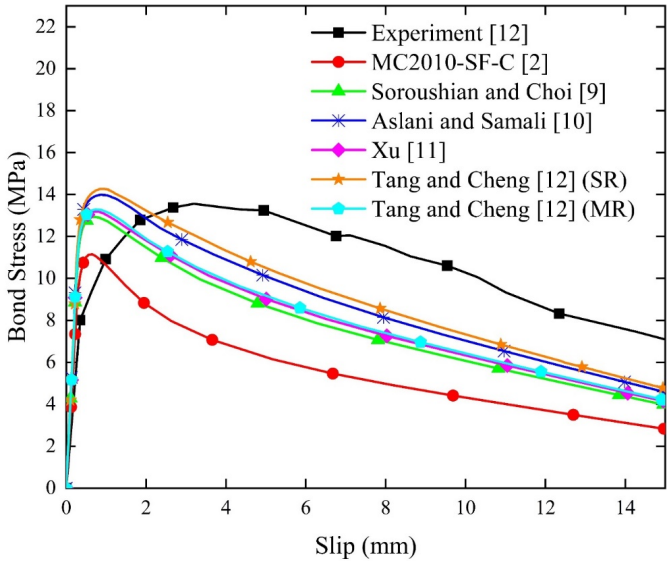

Figure 25: Bond Stress Vs Slip for reference specimen C20#8 [12].

Failure modes

The reference specimen C20#8 [12] failed at concrete splitting in the experiment (see Fig. 26 (a)). In FE models developed for all analytical models [2, 9-12], failure has been initiated by splitting followed by pullout failure. For instance, the failure mechanism, at peak resistance, of the FE model developed using the analytical model by Tang and Cheng [12] by multiple regression is illustrated in Fig. 26 (b)-(c). Fig. 26 (b) shows that the surrounding concrete of the bonded region nearly failed due to tension at peak resistance, as the tension damage factor is very close to unity (d_t =0.89). Meanwhile, the scaler stiffness degradation (SDEG) variable of the bonded concrete region, as shown in Fig. 26 (c), was found to be 0.75 at peak, indicating that the border region of the concrete is still not damaged completely. Therefore, pullout failure has not been started at the peak resistance. Furthermore, the contact status of the bonded surface has been checked to ensure the failure mechanism was correct. At peak resistance, where a slip of 0.73 mm occurred, both concrete and rebar regions mostly bonded with each other, as shown in Fig. 27. However, at the final loading stage, i.e., a slip of 15 mm, the bonded portion of rebar has

started to slide over concrete, and some regions have not been in contact with each other, which indicates a partial pullout failure at the end stage.

Fig. 28 shows the nature of crack propagation in reference specimen C20#8. The concrete crack starts to spread radially at the beginning of the analysis when the slip is 0.01mm. However, as it reaches the transverse reinforcement, the crack propagation reduces. At a slip of 0.73 mm, damage was found in the concrete near the bonded area and concrete face. Despite the crack propagation starting at the beginning, the reference specimen still undergoes a 15 mm slip without dropping bond stress altogether.

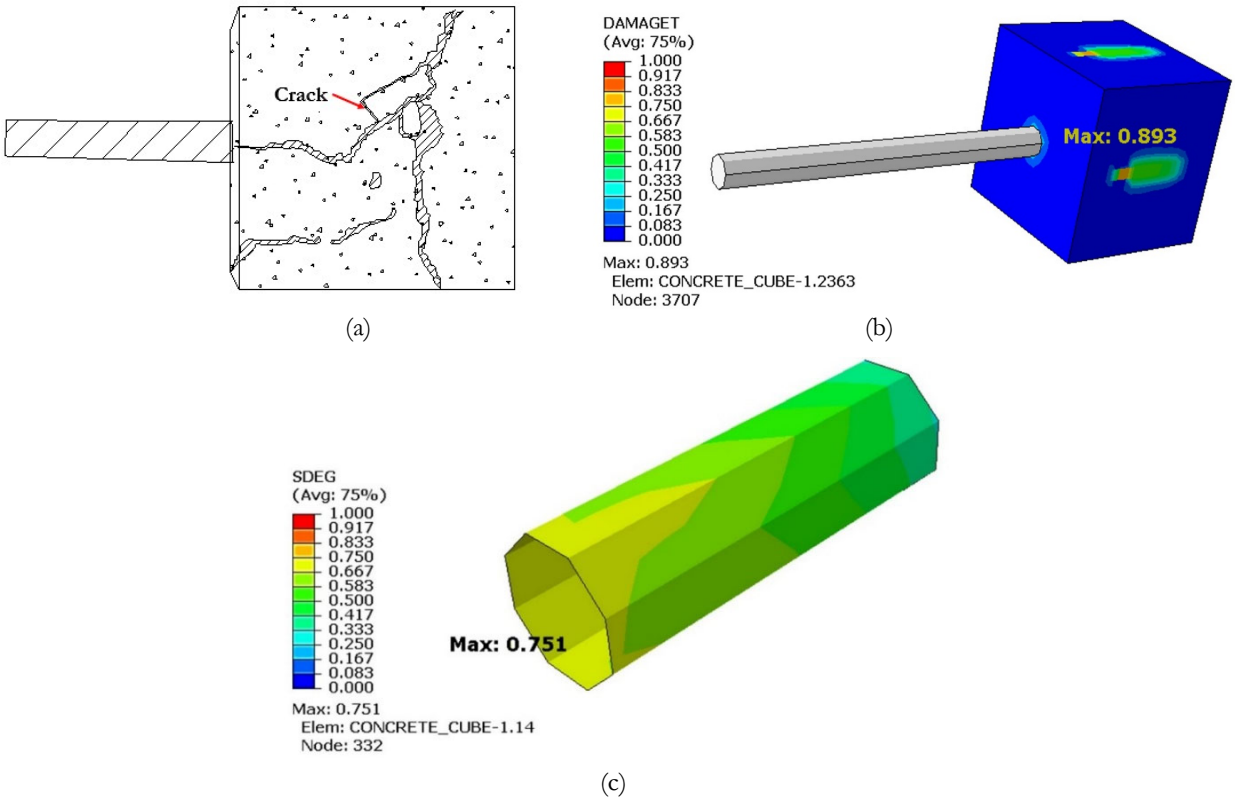

Figure 26: Failure pattern of reference specimen C20#8 [12] (a) experimental (b) damageT output of numerical model (c) SDEG output for concrete-reinforcement bonded region.

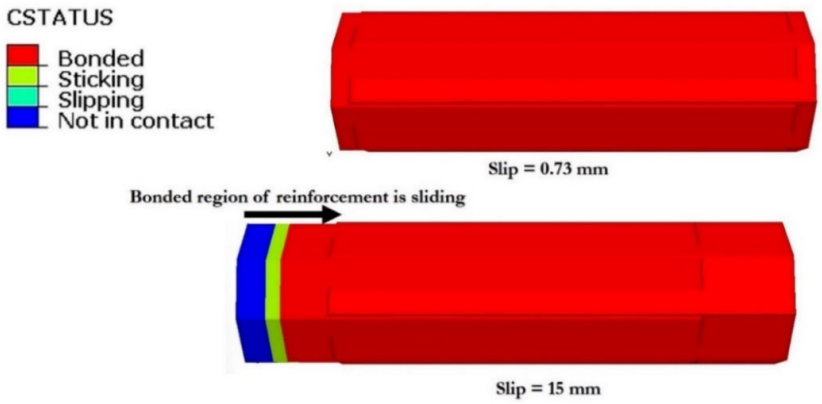

Figure 27: Contact status of bonded region of concrete-reinforcement of reference specimen C20#8 [12].

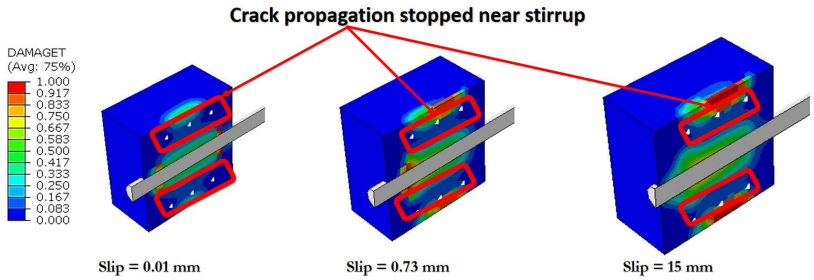

Figure 28: Crack propagation in reference specimen C20#8.

Performance evaluation of the proposed FE modelling strategy and analysis

The performance of the finite element modelling strategy and analysis has been evaluated by comparing the maximum bond stress and failure mechanism in FE analysis with that of in reference experiments. The maximum bond stresses and failure mechanisms of the reference specimens in the experiment and FE analysis are summarized in Tab. 7. In addition, the ratio of the experimental to FE maximum bond stresses, along with the failure mechanism, is shown in Fig. 29. It is evident that the developed FE models could predict the maximum bond stresses fairly in most of the reference specimens except the reference specimen that have cover to depth ratio (c/d) near to 3.41, which has been considered as a margin to have pullout or spitting failure as suggested by Deng et al. [21]. The experimental to FE maximum bond stresses ratio was in a range of 0.85 ~ 1.22, except for the aforementioned reference specimen. Notably, the maximum bond stresses of the reference specimens with experimental pullout, splitting with confinement, and combined failure could be estimated closely by the analytical models suggested by Sturm & Visintin [3], Tang and Cheng [12], Esfahani and Rangan [4], respectively with experimental to FE maximum bond stresses ratio of 0.97, 1.02 and 1.00, respectively. In addition, the developed FE models could predict the failure mechanisms correctly when c/d is less than 3.41, below which splitting or combined failures were observed in experiments.

Reference Specimen	Experimental		Finite Element Analysis			$\frac{\tau_{max,exp}}{\tau_{max,FEM}}$
	Observed Failure Mode	Observed τ_{max} (MPa)	Adopted Models	FEM τ_{max} (MPa)	FEM Failure	
E1R16	Pullout	18.04	MC2010-PF [2]	20.81	Initiated by splitting, followed by partial pullout	0.87
			Sturm and Visintin [3]	18.64	Initiated by splitting, followed by partial pullout	0.97
			Esfahani and Rangan [4]	21.30	Steel Yielded	0.85
			Harajli et al. [5]	21.30	Steel Yielded	0.85
			Huang et al. [6]	21.19	Steel Yielded	0.85
C1R20	Splitting	17.48	MC2010-SF [2]	7.73	Initiated by splitting and followed by complete pullout	2.26
			Sturm and Visintin [3]	10.99	Initiated by splitting and followed by complete pullout	1.59

Reference Specimen	Experimental		Finite Element Analysis			$\frac{\tau_{max,exp}}{\tau_{max,FEM}}$
	Observed Failure Mode	Observed τ_{max} (MPa)	Adopted Models	FEM τ_{max} (MPa)	FEM Failure	
E1R16-60	Pullout+ Splitting	11.69	Harajli et al. [5]	11.96	Initiated by splitting and followed by complete pullout	1.46
			Oragun et al. [7]	8.88	Initiated by splitting and followed by complete pullout	1.97
			Hadi [8]	7.02	Initiated by splitting and followed by complete pullout	2.49
			MC2010-SF [2]	9.58	Initiated by pullout however followed by splitting	1.22
			Sturm and Visintin [3]	12.20	Initiated by pullout however followed by splitting	0.96
			Esfahani and Rangan [4]	11.65	Initiated by pullout however followed by splitting	1.00
			Harajli et al. [5]	12.31	Program terminated by convergence error	0.95
			Huang et al. [6]	12.29	Program terminated by convergence error	0.95
			Oragun et al. [7]	9.74	Initiated by pullout however followed by splitting	1.20
			Hadi [8]	9.79	Initiated by pullout however followed by splitting	1.19
C20#8	Splitting	13.58	MC2010-SF-C [2]	11.16	Initiated by splitting however followed by partial pullout	1.21
			Soroushian and Choi [9]	12.94	Initiated by splitting however followed by partial pullout	1.05
			Aslani and Samali [10]	13.99	Initiated by splitting however followed by partial pullout	0.97
			Xu [11]	13.19	Initiated by splitting however followed by partial pullout	1.03
			Tang and Cheng [12] by simple regression	14.27	Initiated by splitting however followed by partial pullout	0.95
			Tang and Cheng [12] by multiple regression	13.29	Initiated by splitting however followed by partial pullout	1.02

Table 7: Comparison of maximum bond stress and failure pattern of all reference specimens [12,21].

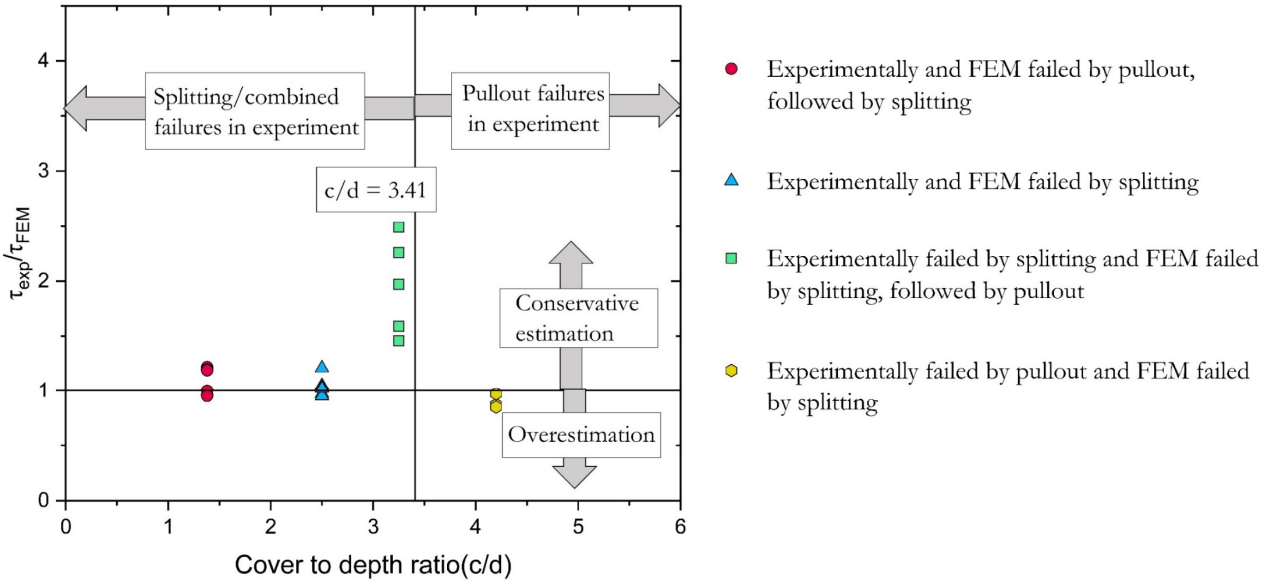

Figure 29: Comparison of bond stress between numerical and experimental results.

CONCLUSION

This study aimed to develop an FE modelling strategy and to conduct a FE analysis of RC pullout specimens to predict the bond-slip relationship of steel and concrete using the surface-based cohesive interaction feature of ABAQUS. In FE models, several analytical models [2-12] were utilized as input for the bond stress-slip behavior of steel-concrete. The effectiveness of the proposed finite element modeling strategy and FE models was then investigated by comparing the experimental results of Deng et al. [21] and Tang and Cheng [12] in terms of bond-slip curves and failure patterns. The following conclusions can be outlined from the limited scope of this study:

- The proposed finite element strategy and models have the capability to predict the bond-slip behavior in elastic regions accurately.
- The proposed finite element strategy and models showed satisfactory results regarding maximum bond stress for most of the reference pullout specimens, except for specimens (without confining reinforcement) that failed by splitting in reference experiment. FE models with analytical models of Sturm and Visintin [3], Esfahani and Rangan [4], and Tang and Cheng [12] have predicted maximum bond stress with 96.7%, 99.7%, and 97.9% accuracy when compared to experimental results of reference specimens with pullout, splitting-pullout, and splitting (with confining reinforcement) failure, respectively.
- The developed FE models captured the crack propagation and failure mechanisms of reinforcement and concrete under the pullout test.

This FE analysis has scopes for further improvement. The proposed FEM strategy has a limitation in predicting the maximum bond stress of pullout specimens (without confining reinforcement) that are expected to have a splitting failure. Furthermore, the softening region of bond-slip curves could not be captured precisely, which could be a crucial factor for ductility-based design. These limitations need to be resolved in future studies.

REFERENCES

[1] Tastani, S.P. and Pantazopoulou, S.J. (2010). Direct tension pullout bond test: Experimental results. Journal of Structural Engineering, 136(6), pp. 731-743. DOI: 10.1061/(ASCE)ST.1943-541X.0000159.
[2] CEB. CEB-FIP Model Code 2010; CEB: Lausanne, Switzerland (2010).
[3] Sturm, A.B. and Visintin, P. (2019). Local bond slip behavior of steel reinforcing bars embedded in ultra high performance fibre reinforced concrete. Structural Concrete, 20(1), pp. 108-122. DOI: 10.1002/suco.201700149.

[4] Esfahani, M.R. and Rangan, B.V. (1998). Bond between normal strength and high-strength concrete (HSC) and reinforcing bars in splices in beams. Structural Journal, 95(3), pp. 272-280. DOI: 10.14359/545.
[5] Harajli, M.H., Hout, M. and Jalkh, W. (1995). Local bond stress-slip behavior of reinforcing bars embedded in plain and fiber concrete. Materials Journal, 92(4), pp. 343-353. DOI: 10.14359/999.
[6] Huang, Z., Engström, B. and Magnusson, J. (1996). Experimental investigation of the bond and anchorage behaviour of deformed bars in high strength concrete. Chalmers University of Technology, 95, pp. 4-4.
[7] Orangun, C.O., Jirsa, J.O. and Breen, J.E. (1977). A reevaulation of test data on development length and splices. In Journal Proceedings, 74(3), pp. 114-122. DOI: 10.14359/10993.
[8] Hadi, M.N. (2008). Bond of high strength concrete with high strength reinforcing steel. The Open Civil Engineering Journal, 2(1), pp. 143-147.
[9] Soroushian, P. and Choi, K.B. (1989). Local bond of deformed bars with different diameters in confined concrete. Structural Journal, 86(2), pp. 217-222. DOI: 10.14359/2731.
[10] Aslani, F. and Nejadi, S. (2012). Bond behavior of reinforcement in conventional and self-compacting concrete. Advances in Structural Engineering, 15(12), pp. 2033-2051. DOI: 10.1260/1369-4332.15.12.2.
[11] Xu, Y.L. (1997). Simplified model of bond-slip constitutive relationship of reinforced concrete. Eng. Mech, 2, pp. 34-38.
[12] Tang, C.W. and Cheng, C.K. (2020). Modeling local bond stress–slip relationships of reinforcing bars embedded in concrete with different strengths. Materials, 13(17), p. 3701. DOI: 10.3390/ma13173701.
[13] Burdziński, M. and Niedostatkiewicz, M. (2022). Experimental-Numerical Analysis of the Effect of Bar Diameter on Bond in Pull-Out Test. Buildings, 12(9), p. 1392. DOI: 10.3390/buildings12091392.
[14] Abbas, N., Yousaf, M., Akbar, M., Saeed, M.A., Huali, P. and Hussain, Z. (2022). An experimental investigation and computer modeling of direct tension pullout test of reinforced concrete cylinder. Inventions, 7(3), p. 77. DOI: 10.3390/inventions7030077.
[15] Beliaev, M., Semenov, A., Semenov, S. and Benin, A. (2016). Simulation of pulling the reinforcing bar from concrete block with account of friction and concrete damage. In MATEC Web of Conferences, 73, 04010. EDP Sciences. DOI: 10.1051/matecconf/20167304010.
[16] Murcia-Delso, J. and Benson Shing, P. (2015). Bond-slip model for detailed finite-element analysis of reinforced concrete structures. Journal of Structural Engineering, 141(4), p. 04014125. DOI: 10.1061/(ASCE)ST.1943-541X.000107.
[17] Cairns, J. (2021). Local bond–slip model for plain surface reinforcement. Structural Concrete, 22(2), pp. 666-675. DOI: 10.1002/suco.202000114.
[18] Tabatabaei Mirhosseini, R., Araghizadeh, E. and Rashidi, S. (2023). Approximate Relationship for the Bond-Slip Using a Concrete Damage-Plastic Model. Advances in Materials Science and Engineering, 2023. DOI: 10.1155/2023/1320192.
[19] Luna Molina, F.J., Fernández Ruiz, M.A., Hernández Montes, E. and Alonso Alonso, M.C. (2015). Bond strength of galvanized steel: experimental and numerical study based on pull-out tests. In 3rd International Conference on Mechanical Models in Structural Engineering, 143-158. Sevilla, España: CMMoST 2015. Víctor Compán Cardiel [etc.].
[20] Valente, M. (2012). Bond strength between corroded steel rebar and concrete. International Journal of Engineering and Technology, 4(5), p. 653. DOI: 10.7763/IJET.2012.V4.454.
[21] Deng, M., Pan, J. and Sun, H. (2018). Bond behavior of steel bar embedded in Engineered Cementitious Composites under pullout load. Construction and Building Materials, 168, pp. 705-714. DOI: 10.1016/j.conbuildmat.2018.02.165.
[22] Lubliner, J., Oliver, J., Oller, S. and Onate, E. (1989). A plastic-damage model for concrete. International Journal of solids and structures, 25(3), pp. 299-326. DOI: 10.1016/0020-7683(89)90050-4.
[23] Lee, J. and Fenves, G.L. (2001). A return-mapping algorithm for plastic-damage models: 3-D and plane stress formulation. International Journal for Numerical Methods in Engineering, 50(2), pp. 487-506. DOI: 10.1002/1097-0207(20010120)50:2%3C487::AID-NME44%3E3.0.CO;2-N.
[24] Lee, J. (1996). Theory and implementation of plastic-damage model for concrete structures under cyclic and dynamic loading. University of California, Berkeley.
[25] Lee, J. and Fenves, G.L. (1998). Plastic-damage model for cyclic loading of concrete structures. Journal of engineering mechanics, 124(8), pp. 892-900. DOI: 10.1061/(ASCE)0733-9399(1998)124:8(892).
[26] GB 50010-2010 (2010). Code for design of concrete structures. Standardization Administration of China: Beijing, China.
[27] Shao, S., Wu, Y., Fu, H., Feng, S. and Zhang, J. (2023). Numerical Investigation on the Mechanical Properties of Vault Void Lining and Steel Plate Strengthening. Materials, 16(2), p. 789. DOI: 10.3390/ma16020789.
[28] Rewers, I. (2019). Numerical analysis of RC beam with high strength steel reinforcement using CDP model. In IOP Conference Series: Materials Science and Engineering, 471(2), p. 022025). IOP Publishing.

[29] Guo, Y.B., Gao, G.F., Jing, L. and Shim, V.P. W. (2017). Response of high-strength concrete to dynamic compressive loading. International Journal of Impact Engineering, 108, pp. 114-135. DOI: 10.1016/j.ijimpeng.2017.04.015.
[30] Michal, S. and Andrzej, W. (2015). Calibration of the CDP model parameters in Abaqus. World Congr Adv Struct Eng Mech (ASEM 15), Incheon Korea.
[31] Wosatko, A., Winnicki, A., Polak, M.A. and Pamin, J. (2019). Role of dilatancy angle in plasticity-based models of concrete. Archives of Civil and Mechanical Engineering, 19, pp. 1268-1283. DOI: 10.1016/j.acme.2019.07.003
[32] Niu, Y., Wang, W., Su, Y., Jia, F. and Long, X. (2023). Plastic damage prediction of concrete under compression based on deep learning. Acta Mechanica, pp. 1-12. DOI: 10.1007/s00707-023-03743-8.
[33] Sidoroff, F. (1981). Description of anisotropic damage application to elasticity. In Physical Non-Linearities in Structural Analysis: Symposium Senlis, France May 27–30, 1980 (pp. 237-244). Berlin, Heidelberg: Springer Berlin Heidelberg. DOI: 10.1007/978-3-642-81582-9_35.
[34] Manual, A.B.A.Q.U.S. (2014). ABAQUS 6.14 Analysis User's Manual. Online Documentation Help: Dassault Systemes.
[35] Wriggers, P. and Wriggers, P. , 2006. Discretization, large deformation contact. Computational Contact Mechanics, pp. 225-307. DOI: 10.1007/978-3-540-32609-0_9.
[36] Seok, S., Haikal, G., Ramirez, J.A., Lowes, L.N. and Lim, J. (2020). Finite element simulation of bond-zone behavior of pullout test of reinforcement embedded in concrete using concrete damage-plasticity model 2 (CDPM2). Engineering Structures, 221, p. 110984. DOI: 10.1016/j.engstruct.2020.110984.
[37] Lagier, F., Massicotte, B. and Charron, J.P. (2016). 3D nonlinear finite-element modeling of lap splices in UHPFRC. Journal of Structural Engineering, 142(11), p. 04016087. DOI: 10.1061/(ASCE)ST.1943-541X.00015.
[38] Seok, S., Haikal, G., Ramirez, J.A. and Lowes, L.N. (2018). High-resolution finite element modeling for bond in high-strength concrete beam. Engineering Structures, 173, pp. 918-932. DOI: 10.1016/j.engstruct.2018.06.068.
[39] Idun, E.K. and Darwin, D. (1999). Bond of epoxy-coated reinforcement: coefficient of friction and rib face angle. American Concrete Institute. DOI: 10.14359/698.
[40] Eligehausen, R., Popov, E.P. and Bertero, V.V. (1982). Local bond stress-slip relationships of deformed bars under generalized excitations. DOI: 10.18419/opus-415.
[41] Gan, Y. (2000). Bond stress and slip modeling in nonlinear finite element analysis of reinforced concrete structures (p. 251). Toronto, ON, Canada: University of Toronto.
[42] Henriques, J., da Silva, L.S. and Valente, I.B. (2013). Numerical modeling of composite beam to reinforced concrete wall joints: Part I: Calibration of joint components. Engineering Structures, 52, pp. 747-761. DOI: 10.1016/j.engstruct.2013.03.041.
[43] Keuser, M., Kepp, B., Mehlhorn, G. and Rostasy, F. (1983). Nonlinear static analysis of end-fittings for GFRP-prestressing rods. Computers & Structures, 17(5-6), pp. 719-730. DOI: 10.1016/0045-7949(83)90086-X.
[44] Pauletta, M., Rovere, N., Randl, N. and Russo, G. (2020). Bond-slip behavior between stainless steel rebars and concrete. Materials, 13(4), p. 979. DOI: 10.3390/ma13040979.
[45] Bigaj, A.J. (1995). Bond behaviour of deformed bars in NSC and HSC: Experimental study. Report Stevin Laboratory, Concrete Structures 25.5-95-11.
[46] Lee, S.W., Kang, S.B., Tan, K.H. and Yang, E.H. (2016). Experimental and analytical investigation on bond-slip behaviour of deformed bars embedded in engineered cementitious composites. Construction and Building Materials, 127, pp. 494-503. DOI: 10.1016/j.conbuildmat.2016.10.036.
[47] Malm, R. (2009). Predicting shear type crack initiation and growth in concrete with non-linear finite element method (Doctoral dissertation, KTH).